Summer 6-5-2017

Comprehensive Silica Removal with Ferric Compounds for Industrial Wastewater Reuse

Ehren D. Baca
University of New Mexico

Ehren D. Baca

Candidate

Department of Civil Engineering

Department

This thesis is approved, and it is acceptable in quality and form for publication:

Approved by the Thesis Committee:

Dr. Kerry J. Howe, Chairperson

Dr. Patrick Brady

Dr. Jr-Lin Lin

Dr. Jose Cerrato

Dr. Zachary Stoll

COMPREHENSIVE SILICA REMOVAL WITH FERRIC COMPOUNDS FOR INDUSTRIAL WASTEWATER REUSE

by

Ehren Baca

BACHELOR OF SCIENCE, CHEMICAL ENGINEERING

THESIS

Submitted in Partial Fulfillment of the Requirements for the Degree of

Master of Science

Civil Engineering

The University of New Mexico Albuquerque, New Mexico

July, 2017

Acknowledgements

In completion of this project I would like to acknowledge the following people that contributed to this work. Dr. Kerry Howe for accepting me as a graduate student and providing me guidance and critical review in my proposals and research. My thesis committee, Dr. Patrick Brady, Dr. Jr-Lin Lin, Dr. Jose Cerrato and Dr. Zachary Stoll for their support and feedback on this work. 陳威亦 for his constant assistance and guidance in the lab. My group-mates Lauren Breitner and John Stomp for listening to my research updates and helping me refine my ideas.

Dedication

I dedicate this document to my family, without whom none of this would have been possible. I would like to thank each of you for all that you have done for me. My Wife for being my joy and giving me a reason to be better. My Mom for being my champion and for keeping me in check. My Father for being my teacher and always supporting me, regardless. My big Brother for showing me how to get down and all the chuckles, giggles and missions. My Uncles for their support and helping to facilitate my undergraduate education which allowed me to get to this point. My dogs for more than I can articulate. Finally, all praise and gratitude to the Most High for giving me a shot at this life and for refining me through trials and tribulation- I will get there.

COMPREHENSIVE SILICA REMOVAL WITH FERRIC COMPOUNDS FOR INDUSTRIAL WASTEWATER REUSE

By

Ehren Baca

B.S. Chemical Engineering, University of New Mexico, 2010

M.S. Civil Engineering, University of New Mexico, 2017

Abstract

Cooling towers, integrated circuit (IC) manufacture and reverse osmosis (RO) generate copious amounts of wastewater high in colloidal and reactive silica inhibiting on-site or synergistic reuse of these streams. Silica present in cooling water can reach solubility limits via evaporation and form impervious scale on heat transfer surfaces that decreases efficiency. When water is treated by RO operating at high rejection, silica forms difficult-to-remove scale on the membrane feed side in the form of glassy patches and communities of aggregate particles, inhibiting aspirations for zero liquid discharge. Current methods for silica scale mitigation include abundant dosing with chemical antiscalents or complex operating schemes involving ion exchange for cation removal and large pH swings. This work evaluates the implementation of the common chemical coagulant ferric chloride ($FeCl_3$) and highly insoluble ferric hydroxide ($Fe(OH)_3$) in the removal of silica by coagulation and adsorption mechanisms, respectively. Ferric chloride was optimized for silica colloid coagulation in IC wastewater via charge neutralization resulting in 97.2% turbidity removal. Adsorption of reactive silica on ferric hydroxide using a sequencing batch reactor approach exhibited 94.6% silica removal for

the first adsorption cycle in under 60 minutes. Silica adsorption was found to fit the Langmuir isotherm relationship and was further modeled with surface complexation reactions using PHREEQC. Analytical characterization of adsorbent supernatant and adsorbent material provided evidence of silica polymerization on the iron surface. This work serves to provide a benchmark as a rigorous investigation applying ferric chloride and ferric hydroxide to silica removal in real industrial waste streams. Marrying these compounds together has proven effective for comprehensive silica removal to facilitate industrial wastewater reuse.

Table of Contents

List of Figures

List of Tables

Introduction

In the USA alone, over 160 billion gallons of water is withdrawn per day to accommodate steam generation and cooling processes in thermoelectric power generation (Maupin et al., 2014). A single Integrated circuit manufacture (IC) facility, such as Intel in Rio Rancho New Mexico, uses and discharges upwards of 2 million gallons of water per day during normal processing (Weitz, 2016). The El Paso inland reverse osmosis (RO) desalination facility generating 15 million gallons of potable water per day at 82% water recovery produces 3 million gallons of wastewater concentrate per day (Ning et al., 2010). If these water sources could be reused, within each respective industry or as synergistic feed to other industries, water withdrawal demands could be significantly alleviated and water conservation enhanced. However, silica content is an underlying factor inhibiting reuse of these water streams and preventing high recovery in RO. In the thermoelectric industry water is eventually blowdown and discarded due to exceeding silica content. This is because silica, when present in either boiler or cooling loops, is concentrated by evaporation and can deposit as hard glassy scale on turbine blades, piping, and heat transfer surfaces (Iler, 1974). Silica scale results in decreased efficiency and severely increased operational costs, making blowdown water ineligible for reuse due to its high silica content. Water produced in the integrated circuit industry can contain high concentrations of colloidal and particulate silica from chemical mechanical planarization processes preventing its reuse in industry or reverse osmosis (Chuang et al., 2007). RO, used both in the IC industry to generate ultra-pure water and in desalination to create potable water, is severely hindered by

silica. When silica is concentrated by RO it forms hard glassy scale on the membrane feed side that requires hazardous and costly chemicals to remove (Den and Wang, 2008). Therefore, when silica is present in water subjected to RO, it requires reduced process recovery in an attempt to prevent silica from precipitating. This then produces large waste streams and inhibits aspirations for zero liquid discharge (ZLD). For instance, due to silica, the El Paso desalination facility cannot operate at high recoveries and is forced to deep well inject for waste stream management (Ning et al., 2010). In order to realize effective reuse of industrially generated wastewater from thermoelectric, IC and RO processes, a robust and effective means of silica removal must be developed.

Project Objectives

This work investigates the feasibility of using ferric chloride and ferric hydroxide in comprehensive silica removal from IC and RO industrial wastewater. The proven effectiveness of ferric chloride as a coagulant in water treatment warrants its plausibility as an effective coagulant for removal of silica colloids in integrated circuit wastewater. Ferric hydroxide, formed by reacting ferric chloride and sodium hydroxide, has a known affinity for silica adsorption (Iler, 1974). Also, the robust insolubility of ferric hydroxide makes it ideal to adsorb silica in a variety of water conditions without the risk of liberating metal cations into subsequent process streams. Objectives of this study include the following:

1. Determine optimal $FeCl_3$ dose and mechanism for coagulation in IC wastewater
2. Determine $Fe(OH)_3$ adsorption rates and mechanism for dissolved silica adsorption
3. Compare effectiveness of sequencing batch reactor and equilibrium adsorption

Background

The effects of silica scale are by no means new to the power production and reverse osmosis industries. Silica defined itself as a problematic constituent early in boiler and turbine applications when it began to deposit on turbine blades, inside of plumbing, and on heat transfer surfaces as impervious glassy scale (Iler, 1979). This occurs when silica is subjected to volatilization due to extreme temperatures and pressures or becomes concentrated by evaporation and exceeds its solubility limits (Iler, 1979). The result is turbine imbalance, flow restriction, decreased heat transfer efficiency and increased operational cost. In RO, silica can form debilitating scale on the membrane feed side. This is caused by the selective flux of water through the membrane, concentrating silica and forming particle aggregates and hard glassy patches (Den and Wang, 2008). RO fouling leads to increased operational pressure, decreased specific flux, lowered efficiency and increased cost (Ning, 2010). For boiler feed water, the most comprehensive and complete answer to silica scale formation is silica removal (Iler, 1979). Silica removal has been around for many years and is often comprised of ion exchange. For cooling water and reverse osmosis on the other hand, mitigation techniques remain the dominant means to preserve processes from silica scale formation. Mitigation techniques leverage the physiochemical properties of silica in solution and rely on abundant chemical additives to kinetically prevent polymerization.

Silica on the Earth

Silica is a prolific constituent of the Earth's crust which is attributed to be 95% silicate material (Shipman et al., 2016). The orthosilicate anion (SiO_4^-) is the primary building block for silicate formation. With 4 valence electrons, similar to carbon, Silicon has a

high affinity to bond with oxygen and metal ions to form silicates. Siloxane (Si-O-Si) bonds are the strongest and most stable bonds silicon can make, but it is also common to have bonding with metals (Si-O-M). The predominant form of silica found on earth is crystalline silica $(SiO_2)_x$ known as quartz (Eikenberg, 1991). River waters typically range from 5-35 mg/L dissolved silica content depending on location (Iler, 1979). When river waters reach the sea or areas of high salinity their dissolved silica concentration decreases to 5-15 mg/L due to salting out effects (Iler, 1979). Ground water in New Mexico can contain anywhere from 30 mg/L to 70 mg/L dissolved silica. Mineral silicates, which are the source of dissolved silica in all water sources, exist in 5 primary crystalline arrangements. Each arrangement of the orthosilicate tetrahedron provides unique mineral characteristics and properties.

Isolated Tetrahedron

Silicon's 4 valence electrons covalently bond with four oxygen atoms creating a tetrahedron structure. This structure, known as the orthosilicate anion, has an overall charge of -4 giving it an affinity to bond with multivalent cations like Mg^{2+}, $Fe^{2+}$and Mn^{2+} (Egger, 2017). These metal cations act as a bridge between negatively charged silicate ions creating a category of minerals called Olivines. Olivines are the most predominant metal-silicates on Earth and their color depends on the cations integrated in their structure (Iler, 1970). Fosterite (Mg_2SiO_4) for example is clear, Fayalite ($Fe_2SiO_{4)}$ is dark red, and Tephorite (Mn_2SiO_4) exists as varying shades of brown. The characteristic olive green color for which the name 'Olivine' is derived is produced when both Mg^{2+} and Fe^{2+} are included at varying ratios in the silicate mineral.

Chain Tetrahedra

When the orthosilicate anion polymerizes in a linear fashion it can create a chain of tetrahedra (Egger, 2017). These chains, sharing a covalently bonded oxygen atom between them, maintain a negative charge. In order to create a stable mineral, a cation bridge between linear polymorphs is required. This results in rows of tetrahedra sandwiching rows of metal ions. These metal ions, which are ionically bonded and not as strong as the siloxane bonds, create a distinct cleavage plane in the mineral. Two tetrahedra sharing an oxygen atom sandwiching metal cations produces the mineral category called Pyroxenes (Egger, 2017). Pyroxenes are also very common on Earth and predominantly bond with Ca^{2+}, Fe^{2+}, Mn^{2+}, and Mg^{2+} or combinations of each. Example formulas are $(CaFe)_2Si_2O_6$, or $Mg_2Si_2O_6$. Sodium Pyroxenes also exist which accommodate a combination of a trivalent metal and sodium ions such as $NaAlSi_2O_6$.

Double Chain Tetrahedra

When polymerization leads to an arrangement of parallel chain tetrahedra sharing oxygen atoms, a double chain tetrahedra is formed (Egger, 2017). Since the double chain maintains a negative charge, metal cations are once again required to adhere the chains together to form a stable mineral. Double chain tetrahedra silicates are called Amphiboles and host a larger variety of cations (Egger, 2017). For example, the amphibole Holmquistite has the formula $Li_2Mg_3Al_2Si_8O_{22}(OH)_2$.

Sheet Silicates

Continued polymerization of siloxane in a single plane creates a silica sheet (Egger, 2017). Silica sheets are sandwiched together by metal oxide sheets and water

molecules. These components result in perfect and easily sheer-able planes. Silicate sheets are categorized as Micas or Clays. Micas cleave in complete sheets and retain their structure. Clays can accommodate abundant amounts of water, sheer vary easily and do not retain their physical structure. This property makes clays very slippery and highly workable. When clays are heated, as in kilning, the water that was previously providing lubricity between silicate sheets is evaporated leaving a hard and brittle material.

Framework Silicates

Framework silicates maintain siloxane bonding in all directions and do not require cation bridges. For this reason, they are not susceptible to cleavage. Framework silicates constitute a more durable material and their purest form is crystalline SiO_2 called Quartz. Quartz with minor impurities, called isomorphous replacements, produces minerals of varying pigmentation. An example of a famous form of quartz with slight impurities is flint, which has been used throughout human history as a tool due to its strong crystalline structure. Aluminum often takes the place of silica atoms in the silica framework creating the mineral category known as Feldspars (Egger, 2017). Since Aluminum, Al^{3+}, has one more valence electron than Silicon, Si^{4+}, it allows Feldspars to accept another single charged cation. An example of a Feldspar is potassium feldspar, $KaAlSi_3O_8$.

Silicate Weathering

Weathering is the process where silicates are broken down to smaller physical portions or their fundamental chemical constituents. This process can proceed via mechanical,

biological and chemical weathering (Chorley et al., 1964). Mechanical weathering cracks rocks into smaller portions by temperature variations or physical forces. As temperature fluctuates from hot to cold, silicates expand and contract stressing their cleavage planes. If temperature change is rapid enough, fracturing of the silicate can occur. When water or condensation collects in these fractures, freezing causes expansion producing a physical force that perpetuates already existing fractures. Biological weathering proceeds similar to mechanical weathering as roots force their way into rock formations creating larger fractures as they grow. Chemical weathering involves the interface between water and the silicate mineral spurring reactions on the exposed silicate surface. When acidic water interacts with silicon-oxygen-metal bonds on a silicate surface, dissolution can liberate silicic acid from the mineral. An example of this is CO_2 dissolution into surface or ocean water decreasing pH and accelerating silicate weathering (Brady, 1994). This is how CO_2 concentration in the atmosphere, and consequently climate change, is intertwined with rock weathering on the Earth's surface. When silica is leached by acidic water, multivalent metals such as Iron, Aluminum and Magnesium remain in the soil making Laterites, Oxisols, and Ultisols. Plants can also play a role in chemical weathering as their root systems or decaying mass can secrete organic acids, tannins and catechols. Catechols can dissolve silica in neutral conditions without the need for organic and carbonic acids (Iler, 1979). Higher rates of vegetation turnover in hot humid areas has caused higher concentration of weathered soils, such as Oxisols and Ultisols, in places like the Southern USA, Hawaii, ares of South America, and Taiwan. Olivines have been shown to have the highest weathering potential and Framework silicates the least (Chorley et al., 1964).

Silica Dissolution

As described by Iler (1979) dissolution of quartz or massive silica requires a catalyst to proceed. Most commonly hydroxyl ions, but also fluoride ions, serve as the catalyst to liberate silicic acid from solid silica in solution. In water, the surface of $(SiO_2)_x$ is covered with silanol (Si-O-H) groups. As hydroxyl ions in solution approach the bulk silica surface they chemisorb to surface silicon atoms. These chemisorb sites increase the silicon atom coordination number, thereby weakening its bonds with the surrounding oxygen atoms in the mineral. This allows for monomeric silica to be liberated from the bulk material. This proposed reaction mechanism requires the addition of 3 water molecule to complete (Figure 1).

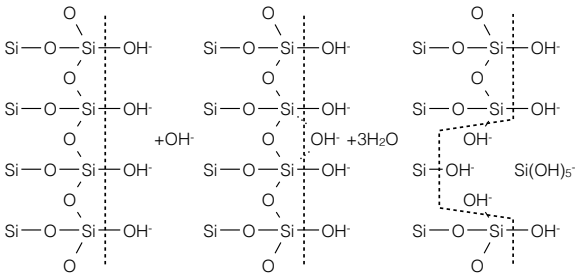

Figure 1. Dissolution of Silica with OH^- as a catalyst. Reproduced from Iler (1979).

Dissolution of amorphous SiO_2 proposed by (Milne et al., 2014) proceeds in a similar fashion. Both quartz and amorphous silica reactions require catalysis via a hydroxyl ion and 3 water molecules. It is interesting to note, however, that these surface dissolution models are not represented by the dissolution reaction. Where the visual surface dissolution models account for a hydroxyl catalyst and 3 waters, the written chemical reaction only requires two waters to balance. This is because the silica surface hydroxyls and siloxane bonds cannot be easily accounted for in a written balanced

equation. The generally accepted written chemical reaction for dissolution of silica proceeds as follows described by Iler (1979):

(1) $(SiO2)_x + 2H_2O \leftrightarrow (SiO2)_{x-1} + Si(OH)_4$

Molybdate and Silica Interaction

The solubility of silica in pure water has been determined over the years by numerous researchers. Typically, characterization of SiO_2 dissolution is done by colorimetric molybdate testing. As SiO_2 dissolves, reactive silica (H_4SiO_4) is produced. The Molybdate reagent rapidly complexes with both reactive silica and phosphate in acidic conditions producing molybdosilicate acid and phosphomolybdic acid. Both produce a yellow color in solution so citric acid is typically used to destroy all phosphomolybdic acid present. Concentration of reactive silica in solution can then be determined by colorimetry where silica concentration is proportional to absorbance. The silicic acid and molybdate reaction as proposed by Iler (1979) is as follows:

(2) $7Si(OH)_4+12H_6Mo_7O_{24}\bullet4H_2O +174H_2O \leftrightarrow 7H_8Si(Mo_2O7)6\bullet28H_2O$

Differing from these reactions are those proposed by HACH Corporation (USA), the manufacturer of the colorimetric device used in this work.

(3) $H_2SiO_3 + 3H_2O \leftrightarrow H_8SiO_6$

(4) $H_8SiO_6 + 12(NH_4)_2MoO_4 + 12H_2SO_4 \leftrightarrow H_8Si(Mo_2O_7)_6 + 12(NH_4)_2SO_4 + 12H_2O$

The reactions proposed by HACH (USA), account for metasilicic acid (H_2SiO_3) as the primary form of dissolved silica in solution. Contrary to this, and predominantly in literature, silicic acid is attributed to protonation of the orthosilicate ion, SiO_4^{4-}, and has been found to exclusively form H_4SiO_4 in solution (Iler, 1979; Sjöburg, 1996; Eickenberg, 1990; Bremere et al., 2000; Chan, 1989; Dietzel, 2002; Hansen et al., 1994) and many more. Nonetheless, the silica-molybdate reaction is an effective means to characterize silicic acid in solution. An interesting observation is that molybdate testing is typically considered to only be effective for the determination of reactive silica in solution and not for determining particulate or colloidal silica matter. However, Okamoto (1959) showed that by increasing molybdate reaction time, massive silica will slowly dissolve into solution forming monomeric silica, increasing color intensity as more complexes are formed. This method, if properly developed, may be a means to apply molybdate testing to quantify silica concentration in solutions with both dissolved and particulate silica.

Physiochemical Properties of Silica

Silica scale mitigation techniques involve pH manipulation to increase solubility, removal of other constituents in solution that decrease silica solubility, and utilization of chemical dispersants to prevent polymerization and precipitation. Effective mitigation of scale by pH manipulation and salt removal can be understood by discussion of silica solubility, speciation and polymerization. Chemical dispersants however, are often proprietary blends and little is disclosed to the public about their chemical makeup.

Solubility

Understanding the solubility of amorphous silica is useful to determine the operational conditions in which silica scale can be prevented. Solubility of amorphous silica and quartz has been abundantly studied over the years and a compilation of equilibrium solubility constants (K_{sp}) were synthesized and presented by Eikenberg (1990). For amorphous silica, pK_{sp} values range from 2.60 (151 mg/L) to 3.02 (57.3 mg/L) (Eikenberg, 1990). Quartz has a lower solubility with pK_{sp} values ranging from 3.74(11 mg/L) to 4.00(6 mg/L) (Eikenberg, 1990). Although the solubility limit for quartz is significantly lower than that of amorphous silica, it requires long periods of time for crystallization to occur (Iler, 1979). This is known as Ostwald's step rule which describes that least stable polymorphs condense first in a saturated solution. Therefore, precipitants of silica in working solutions are almost always amorphous. As described by the silica dissolution reaction (Iler, 1979), solubility of silica is a function of hydroxyl groups in solution. Once liberated from the bulk SiO_2 surface, monomeric silica exists stable in solution for long periods of time below 100 ppm (Iler, 1979). As solution pH increases, monomeric silica de-protonates twice in the range of pH 0-14 and is therefore treated as a diprotic acid as reported by Milne et al., (2014):

(5) $H_4SiO_4 \rightarrow H_3SiO_4^- + H^+$ $pKa_1 = 9.86$

(6) $H_3SiO_2^- \rightarrow H_2SiO_4^{2-} + H^+$ $pKa_2 = 13.14$

Below the pK_{a1}, monomeric silica is the predominant species in solution and therefore more susceptible to precipitation in super saturated conditions. After pK_{a1}, dissolved

silica is de-protonated to $H_3SiO_4^-$ decreasing H_4SiO_4 concentration thereby increasing solubility. The relationship between protonated and deprotonated silica species is illustrated in Figure 2. Ratios of dissolved silica speciation in the pH range of 5.5-10.5 can be seen in Table 1.

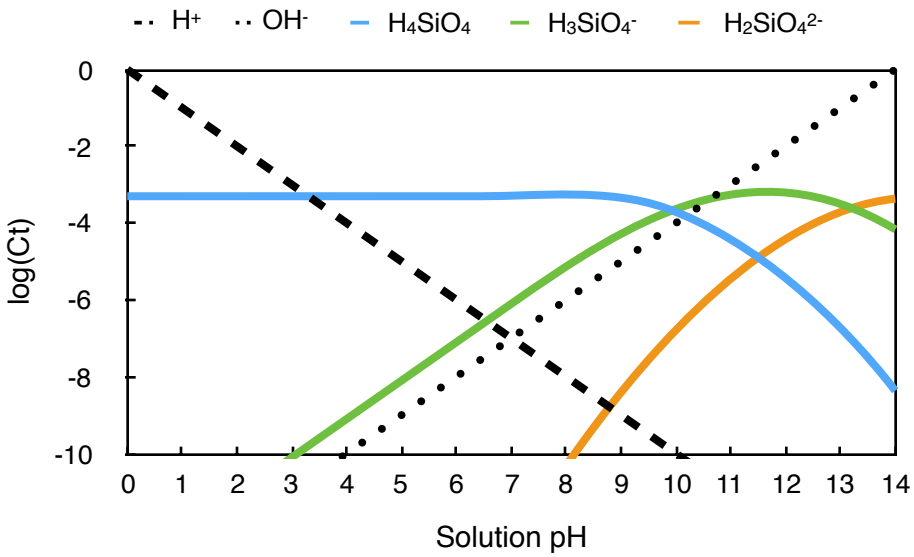

Figure 2. PC-PH diagram of 120 mg/L monomeric silica in solution.

Table 1. Speciation of silicic acid at different pH

pH	$\%H_4SiO_4$	$\%H_3SiO_4^-$	$\%H_2SiO_4^{2-}$
5.5	99.99	0.01	0.00
6.5	99.95	0.05	0.00
7.5	99.50	0.50	0.00
8.5	95.23	4.77	0.00
9.5	66.61	33.38	0.01
10.5	16.61	83.23	0.17

From data generated in pure water experiments, a theoretical solubility diagram of amorphous silica using a pK_{sp} of 2.71 can be derived (Figure 3). For this figure, solubility of amorphous silica was chosen to be 120 mg/L. From acidic ranges to about

pH 9.5, monomeric silica exists protonated at or below its solubility limit. As pH reaches the pKa_1 of silicic acid, solubility increases dramatically.

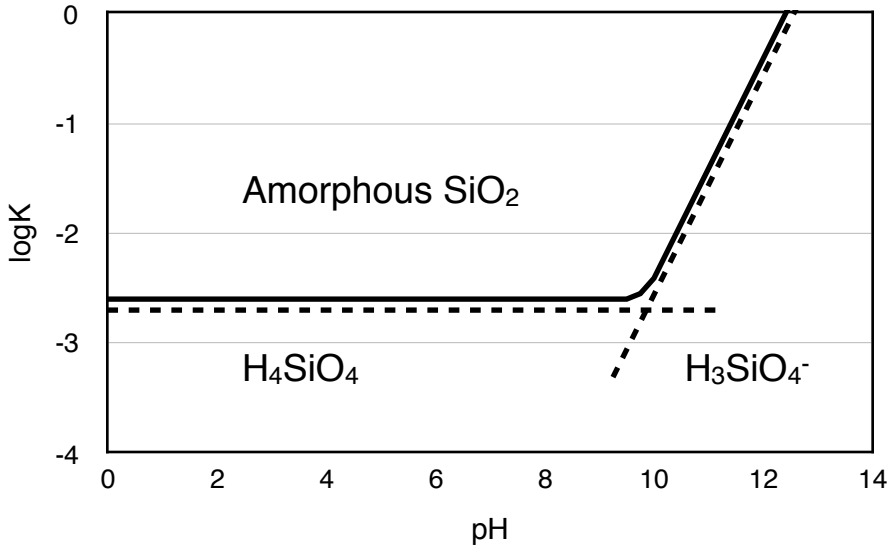

Figure 3. Silica solubility in solution of varying pH

Effect of Salts on Solubility

Although silica solubility increases with pH in pure solutions, when metal salts are present, increasing pH increases the formation of metal silicates (Sheikholeslami et al., 2001). At neutral pH, silica solubility decreases with increasing salt concentration (Milne et al., 2014). Studies conducted by Chen and Marshal (1982) evaluated influence of MgCl, $MgSO_4$, LiCl, $LiNO_3$, NaCl, $NaNO_3$, $NaSO_4$, KCl, KNO_3 on silica solubility. The batch studies were executed over the temperature range of 25-300˚C with varying salt concentration from 0-2 molar. The data was found to fit the Stentchenow equation (Equation 7) with an average standard deviation of 17% (Chan, 1989).

$$Ksp_s = \frac{Ksp}{10^{DM}} \quad (7) \quad \text{(Chan, 1989)}$$

Ksp_s is the solubility of silica in the presence of salt, Ksp is the solubility of silica in a pure solution, D is the Stentchenow parameter which varies for each salt in solution, and M is the molarity of the solute. Utilizing Equation 7, a plot of resulting silica solubility with varying salt molarity was generated (Figure 4). $MgCl_2$ produces the largest decrease in silica solubility with KNO_3 producing the least.

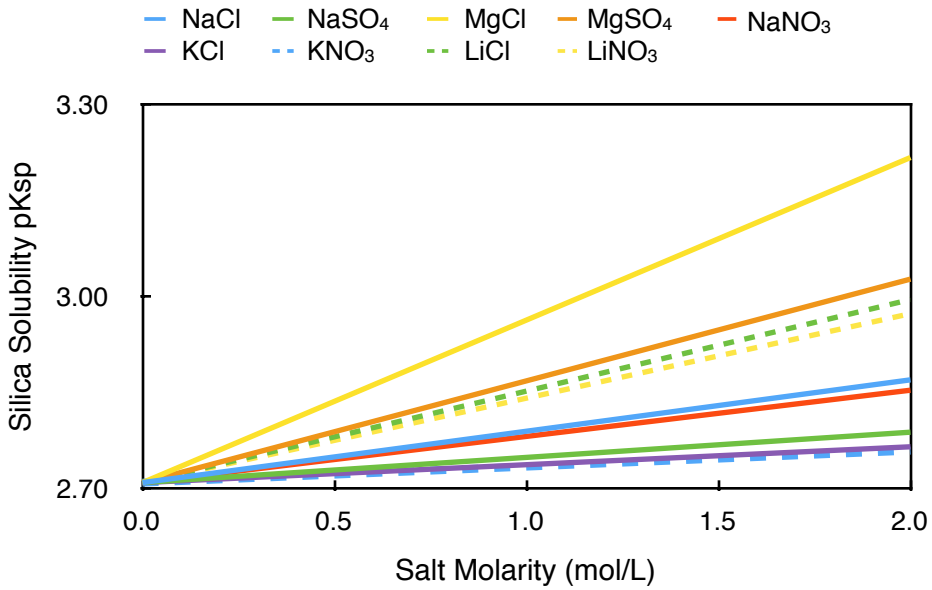

Figure 4. Decreasing solubility of silica in solution as determined by relationship proposed by Chan (1989).

Silica Polymerization

Silica polymerization is important because it provides insight into the initial stages of scale formation when silica has reached its solubility in solution. Monomeric silica will never polymerize as long as its concentration is below the solubility limit (Okamoto, 1956). As silica concentration increases past its solubility limit, monomeric silica begins to undergo condensation reactions. These reactions proceed differently based on the pH of water, but always serve to increase siloxane (Si-O-Si) bonding. This then dictates

that as silica polymers are formed, they preferentially create ring structures to decrease silanol (Si-O-H) groups. Dimerization is the first phase in this process, although dimer concentration has been found to never exceed 5% in solution (Bremere et al., 2000). Polymerization proceeds until about 3 or 4 silica atoms where the structure begins to form a ring (Bremere et al, 2000). Dimerization and trimerization occurring in neutral conditions below the pK_{a1} of silica proceed as follows:

(8) $H_4SiO_4 + H_4SiO_4 = H_6Si_2O_7 + H_2O$ (Eikenberg, 1990)

(9) $H_4SiO_4 + H_6Si_2O_7 = H_8Si_3O_{10} + H_2O$ (Eikenberg, 1990)

Dimeric silica is a stronger acid than the monomeric silica and de-protonates at pKa_1 8.25.

(10) $H_6Si_2O_7 \leftrightarrow H^+ + H_5Si_2O_7^-$ pK_{a1}= 8.25 (Milne et al., 2014)

Dimerization and trimerization in alkaline conditions above the pK_{a1} of monomeric silica proceed with both protonated and de-protonated monomeric silica species. These reactions may serve to further increase the solubility of silica in solution at high pH.

(11) $H_4SiO_4 + H_3SiO_4^- = H_6Si_2O_7^- + OH^-$ (Milne et al., 2014)

(12) $H_4SiO_4 + H_6Si_2O_7^- = H_7Si_3O_{10} + OH^-$ (Milne et al., 2014)

Polymerization can be effectively characterized experimentally by molybdate testing. This is because, as polymerization increases, monomeric silica concentration decreases which can be detected by colorimetry. Polymerization at pH's below 7 or in the present of salts leads to agglomeration of particles forming precipitous gels (Figure 5). Polymerization at high pH without cations leads to stable suspension of particles (Figure 5). As particles form in pH 7-10 range, in the absence of salts, their growth follows the Ostwald ripening mechanism (Iler, 1979). That is, smaller more soluble particles are dissolved in order to facilitate growth of larger less soluble particles. In supersaturated solutions of pH 7-10, growth up to 10nm occurs rapidly then begins to slow (Iler, 1979). The negative charge associated with these particles at high pH prevents aggregation creating stable colloidal (sol) suspensions. Colloidal suspension can be considered the first step to precipitation of silica in solution (Okamoto et al, 1956). Condensation reactions of silica at pH 7-10 have been found to follow third order kinetics by Okamoto and coworkers (1956).

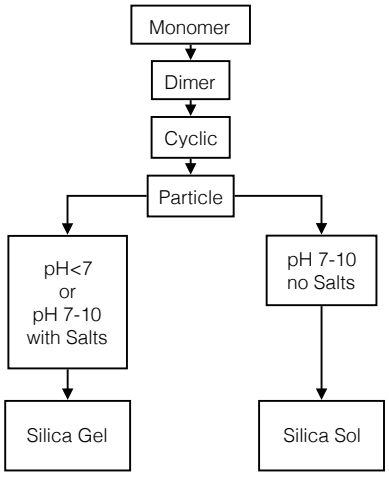

Figure 5. Formation and fate of silica polymers, adapted form Iler (1979), p174

Polymerization Rate

Temperature, pH and the presence of multivalent cations in solution are the largest factors affecting polymerization rate. Increased temperature increases solubility of silica, but can also increase polymerization in saturated solutions (Iler, 1979). Decreasing pH below neutral conditions kinetically hinders silica polymerization resulting in the slowest polymerization rate at pH 3 (Markides et al., 1979). Below pH 3 however, polymerization is catalyzed by H^+ ions and proceeds 10 times faster at pH 1 than at pH 2 (Markides et al.,1979). Above pH 3 polymerization is catalyzed by hydroxyl groups (Iler, 1979) and proceeds 100 times faster at pH 6 than at pH 4 (Markides et al., 1979). Within the range of pH 5.5-9.5, Sheikholeslami and coworkers (2001) found the maximum polymerization rate (<50hours) to be between pH 6.5-8.5, and minimum polymerization rate (>500hours) below pH 5.5 and above pH 9.5. Slow polymerization below pH 5.5 is attributed to solely protonated monomeric silica in solution. This then means that without deprotonated species in solution polymerization proceeds according to Equation 8, which apparently is not as rapid as Equation 11. Slow polymerization above pH 9.5 is attributed to exceeding the pK_{a1} for silica yielding predominantly deprotonated species in solution. This means that protonated silica will be lacking in Equation 11 kinetically hindering polymerization while further deprotonation of silica is simultaneously increasing overall solubility (Sheikholeslami et al., 2001). Since Sheikholeslami and coworkers (2001) observed fastest polymerization between pH 6.5-8.5, they attributed rapid polymerization to the presence of both protonated and deprotonated monomeric silica in solution. Table 1 shows ratios of protonated and deprotonated species existing simultaneously in solution at pH 8.5 which are ~95%

protonated and ~5% deprotonated. Okamoto and co-workers (1956) evaluated polymerization between pH 7-10 and determined a linear trend between pH and the reaction rate constant. This concludes that polymerization above pH 7 is catalyzed by hydroxyl ions (Okamoto, 1959). Chan (1989) reported maximum silica polymerization rate to be in the range of pH 6 to 9.

Effects of Cations on Polymerization Rate

Sheikholeslami and coworkers (2001) investigated the effects of calcium and magnesium on silica polymerization rate. Super saturated solutions of silica were dosed with different amounts of calcium, as well as calcium with magnesium to determine the effect on polymerization. Both calcium and hardness were found to increase polymerization rate with increasing doses. In addition, trivalent ions such as aluminum and iron have been observed to also greatly increase silica polymerization and decrease solubility in solution by forming metal silicates (Iler, 1979), Salvador et al., (2013), Bremere et al., (2000)).

Silica Colloids

Silica colloids are often present in thermoelectric blowdown and IC wastewater and understanding their characteristics is useful for mitigation or removal. The pH corresponding to zero point of charge (pH_{ZPC}) for massive silica and silica colloids in solution is pH 2 (Iler, 1979). As pH increases above or below pH_{ZPC} the particle zeta potential increases or decreases respectively. However, particles below pH 4.5 exhibit neutral to small negative charge and are still susceptible to aggregation with time (Iler, 1979). Above pH 7, colloids increase in stability due to increased magnitude of

repulsion as seen in Figure 5 (Iler, 1979). Presence of multivalent cations in solution will lead to aggregation of stable colloids forming gels (Figure 5).

Silica Scale in Cooling Towers

In thermoelectric power generation the open loop (cooling loop) is susceptible to silica fouling because the water used is typically ground or surface water, both of which contain silica. Open loop water is heated as a result of cooling closed loop boiler feed water, and is itself later cooled by evaporation. Evaporation concentrates silica in solution driving rapid condensation of silica on heat transfer surfaces. When silica scale is allowed to build up over time, heat transfer capability and efficiency of the cooling tower is decreased. Removal of silica scale is a chemically intensive process requiring OH^- of F^- catalysts for dissolution (Figure 1) and is very costly.

Silica Scale Mitigation in Cooling towers

Mitigation of silica scale in cooling waters is typically by proprietary scale inhibitors. NALCO is a popular anti-scalant company that currently has a system in operation at PNM Reeves Generating Station in Albuquerque New Mexico. These additives are called dispersants and serve to keep silica in solution by kinetically hindering silica polymerization and deposition. Since open loop waters must be periodically blown down to maintain low conductivity levels, anti-scalants must be continually added into the process.

Silica Scale in Reverse Osmosis

Reverse osmosis (RO) is often used in the production of ultra-pure water or potable water and can be inhibited by silica scale. Aside from just silica, reverse osmosis is afflicted by many different forms of fouling during normal operation. Due to the nature

of the process, everything that does not diffuse through the membrane will become concentrated on the membrane feed side. Fouling forms from accumulation of biological matter and chemical precipitants as they reach their solubility limits. However, silica scale defines itself as being notoriously difficult to remove once formed requiring hazardous chemical cleaners such as ammonium bifluoride and hydrofluoric acid (Sheikholeslami et al., 2001). Further complicating things, these chemical cleaners also run a significant risk of damaging the RO membrane hindering future use (Sheikholeslami et al., 2001). Silica scale can form by three primary mechanisms on an RO membrane. First, as monomeric silica is concentrated, solubility limits are reached and condensation reactions begin to take place (Equations 8, 9, 11 and 12). These condensation reactions can nucleate on nearby surface sites such as the RO membrane (Sheikholeslami et al., 2001). Or, if concentration is high enough, nucleation can happen spontaneously in solution (Sheikholeslami et al., 2001). Colloids formed in solution impact and imbed on the membrane surface due to high operational pressures (Milne et al., 2014). A third mechanism of scale formation is the aggregation of silica colloids by cations in solution, forming gels. These aggregates deposit and adhere to the RO membrane leading to fouling and further condensation nucleation sites. Sheikholeslami and co-workers (2001) found that water pre-filtered to 5-10 μm was still fouled by silica particles 100-150 μm in size. Therefore, preventing silica from precipitating is the only means to mitigate fouling. This requires operators to limit RO recovery in order to prevent silica from reaching its solubility limits. In RO design, the concentration of solutes at the membrane feed side can be found as a product of the system's rejection and recovery. This relationship is as follows:

$$K_{sp}=C_M=\beta C_F\frac{(1-(1-R)r)}{(1-r)} \quad (13)$$ (Howe et al., 2012)

$$K_{sp}=C_M\beta C_F\left(\frac{1}{1-r}\right) \quad (14)$$ (Simplified, assuming 100% rejection of solutes)

In Equation 14, K_{sp} is the solubility constant of silica in solution, C_M is the concentration of silica at the membrane, β is the concentration polarization factor, C_F is the concentration of silica in the feed, R is the rejection, and r is the recovery. When simplified by assuming 100% rejection of solutes, defining silica concentration (C_f) as a function of pH, and re-arranging to solve for recovery, the resulting equation becomes:

$$r=1-\left[\frac{\beta C_t[H^+]^2}{Ksp\left([H^+]^2+[H^+]K_1+K_1K_2\right)}\right] \quad (15)$$

When plotted, this equation provides a useful visual depiction of the relationship between initial silica concentration and allowable recovery at various pH (Figure 6). With a membrane concentration polarization factor of 1.15, precipitation forms at ~100 mg/L silica as opposed to 120 mg/L, for a solution at pH 7.

Increasing pH decreases protonated monomeric silica, increases solubility and therefore increases allowable recovery. As seen from Figure 6, a solution of pH 11 allows for almost ~95% recovery (in respect to silica fouling) for *pure* solutions up to 100 mg/L. Plotting Equation 15 at different silica concentration while varying pH is represented in Figure 7. As illustrated by Figure 7, all solutions regardless of

concentration, converge on 100% recovery as pH reaches 12. The solubility-pH trends exhibited by Figures 6 and 7 can be leveraged to develop an understanding of silica scale mitigation in RO processing.

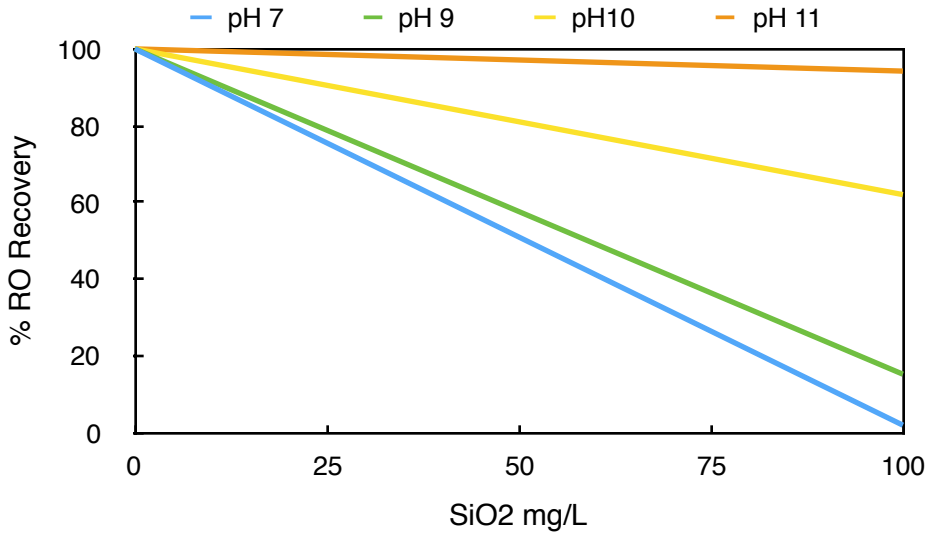

Figure 6. Theoretical decreasing RO rejection with increasing silica concentration

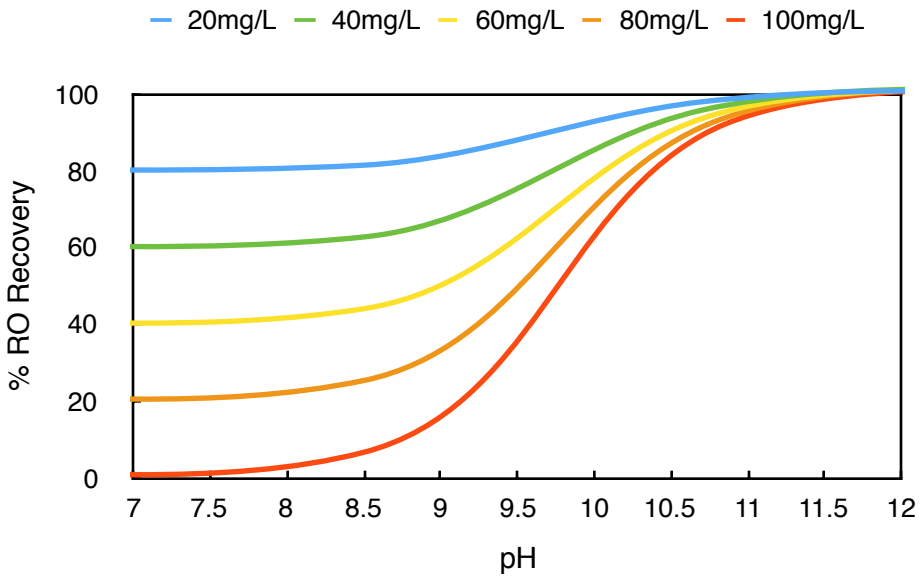

Figure 7. Increasing RO recovery with increasing pH

Influence of Salinity on RO recovery

During RO processing, silica along with other rejected constituents increase in concentration at the membrane feed side. This relationship can be expressed as a combination of Equations 7 and 14 at constant pH.

$$r = 1 - \frac{\beta C_F}{Ksp_S 10^{DM}} \quad (16)$$

Equation 16 was plotted with a constant C_F of 30 mg/L and salt molarity ranging from 0-2 molar (Figure 8). As depicted by the resulting graph, increasing salt concentration decreases available recovery due to a reduction in silica solubility. This data is based on salts evaluated by Chen and Marshal (1982). $MgCl_2$ induces the largest effect on silica solubility of the salts modeled. However, since silica concentration would be increasing simultaneous with salt concentration during actual RO operation, Equation 16 was plotted again with a variable C_F (Figure 9). $MgCl_2$, NaCl, and KCl were evaluated as solutes and increase to a total concentration of 2M. Recovery with no salts present was also plotted as a metric to the effect of salt presence on solubility.

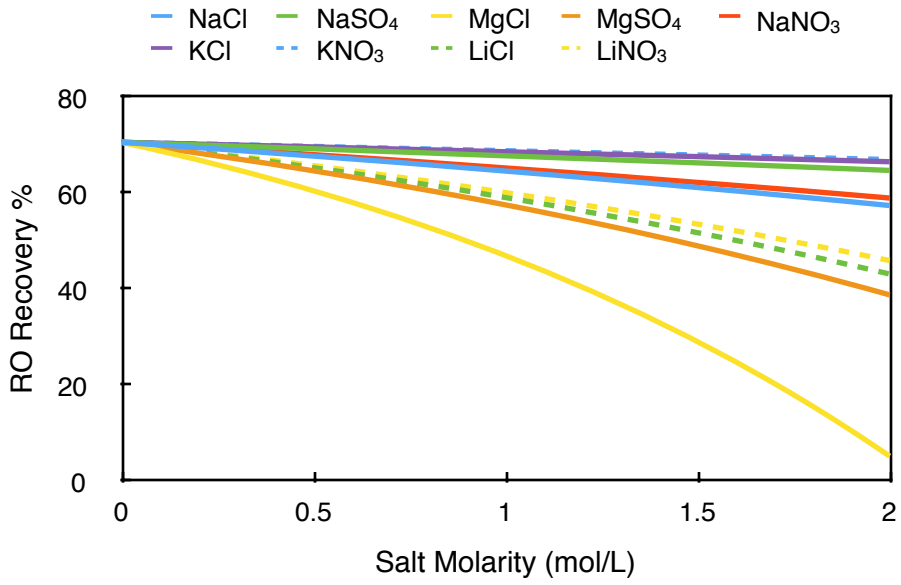

Figure 8. Allowable RO recovery with 30 mg/L silica and increasing salinity

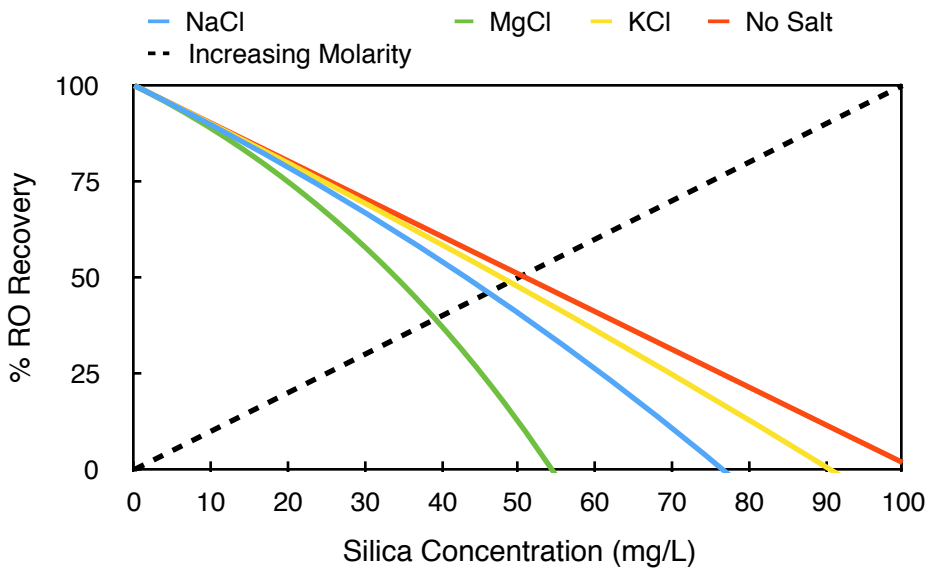

Figure 9. Allowable recovery with increasing silica concentration and salt molarity

Silica Scale Mitigation in RO

Silica scale mitigation in reverse osmosis involves the reduction or elimination of silica scale formation, without the actual removal of silica from water. Mitigation techniques often involve the use of chemical additives that inhibit scale formation during processing. These additives are proprietary blends manufactured by a number of companies such as Lubrizol and King Lee. Exploitation of the pH-solubility relationship of silica is another effective means of mitigating scale formation. As evident in Figure's 6 and 7, increasing pH in pure solutions leads to increased silica solubility and therefore increased water recovery. This characteristic is leveraged in the RO process marketed by GE as HERO (High Recovery Reverse Osmosis) for silica free, ultra-pure water (UPW) production. The HERO process begins with raw water being subjected to weak acid cation exchange to remove calcium and other cations, eliminating the possibility of

precipitating $CaCO_3$ or metal-silicates in subsequent processes (Milne et al., 2014). After ion exchange, the pH is raised above 10.5 and fed to an RO array. At this pH range, in the absences of divalent cations, pure water recovery can exceed 90% without the potential for silica scale formation as shown in Figure 7. This process allows for safe operation of RO to remove silica by increasing solubility and mitigating scale formation. However, chemical usage required for pH adjustment is a significant cost associated with this process. The HERO process was pioneered at the Intel facility in Rio Rancho New Mexico, and still serves as their primary means for generating silica free UPW in the IC industry today. Integral to this process however is the initial removal of hardness cations. With cations present in process water, operation at high pH will inversely lead to increased precipitation of metal silicates and $CaCO_3$ (Sheikholeslami et al., 2002).

An alternative to preliminary ion exchange and high pH is operation below pH 5.5 with cations in solution and a polymerization inhibiting agent (Sheikholeslami et al., 2002). Acidic conditions have been found to kinetically inhibit polymerization of silica and silicates (Markides et al., 1979). Ning and coworkers (2010) investigated RO operation at low pH along with King Lee anti-scalants and reported an achievable recovery of 96% without evidence of fouling.

Silica Removal: Current Approaches

When silica scale mitigation is not an option, or not effective, silica removal can be effective. Silica content in water can have significant impacts in the thermoelectric power generation process in the closed loop water cycle. In high pressure boilers silica solubility increases exponentially and vaporizes with water into the gas phase (Iler, 1979). When the energy contained within high-pressure steam is transferred to

electrical energy via rotation of a turbine, silica in the vapor phase condenses and deposits on the turbine blades eventually impeding flow and causing weight imbalances. Vapor phase silica may also deposit on piping before or after the turbine, restricting flow and decreasing efficiency. Both of these mechanisms can lead to costly damage and even catastrophic failure. The only option to operate boilers and turbines safely is to remove silica from the feed water. Popular methods for silica removal include precipitation, adsorption, ion exchange, chemical coagulation, electrocoagulation and RO. Precipitation, adsorption and ion exchange target removal of soluble monomeric silica (H_4SiO_4). Chemical coagulation and electrocoagulation are effective at removing particulate silica (SiO_2). Reverse osmosis will remove both soluble silica and particulate silica, however often at the expense of the RO membranes unless the HERO process is used. As discussed previously, the HERO process is used specifically to remove silica from IC process water, and silica scale formation is mitigated by process conditions.

Precipitation

Precipitation is considered to be the formation of solids from dissolved solutes in solution. This principal can be leveraged to remove silica via co-precipitation of a metal cation and dissolved silica in solution, forming a metal-silicate (Iler, 1979). Lime softening with soda ash is a vetted water treatment process that has proven effective for monomeric silica removal by metal-silicate precipitation (Al-Mutaz et al., 2004). However, there are a few factors inhibiting wide spread application of this approach. Silica removal by lime softening is reliant on magnesium in solution or requires the addition of magnesium salt. This is because the formation of magnesium-silicates are the critical mechanisms for silica removal. The lime softening reactions are as follows:

(17) $Ca(HCO_3)_2 + Ca(OH)_2 \rightarrow 2CaCO_3 \downarrow + 2H_2O$ (Al-Mutaz et al., 2004)

(18) $Mg(HCO_3)_2 + Ca(OH)_2 \rightarrow CaCO_3 \downarrow + MgCO_3 + 2H_2O$ (Al-Mutaz et al., 2004)

(19) $MgCO_3 + Ca(OH)_2 \rightarrow CaCO_3 \downarrow + Mg(OH)_2 \downarrow$ *$Mg(OH)_2$ adsorbs H_4SiO_4 (Al-Mutaz et al., 2004)

(20) $Mg(HCO_3)_2 + 2H_4SiO_4 \rightarrow MgSi_3O_6(OH)_2 + 6H_2O + 2CO_2$

(Sheikholeslami et al., 2001)

Second, the precipitation of magnesium is reliant on a pH shift to pH 10 or higher, typically 11.5 to 12. If the feed water to a lime softening process is well buffered, it will require abundant addition of lime and caustic in order to achieve the necessary pH (Milne et al., 2014). This leads to the third inhibiting factor which is abundant sludge generation. The sludge produced in lime softening is chemically complex and holds a significant amount of water. Dewatering and disposal of lime sludge is a challenging process that serves to increase operational cost and limit its applicability in industry (Milne et al., 2014).

Adsorption

Adsorption occurs when monomeric silica adheres to insoluble metal hydroxides either formed in solution, or formed previously and added to solution (Iler, 1979). However, it is interesting to note that the actual mechanism of silica adsorption onto a metal hydroxide is still not completely clear (Sheikholeslami et al., 2001). Since dissolved silica often interferes with precipitation of metal hydroxides in solution by forming metal-

silicates (Iler, 1979; Pokravoski et al., 2003), adding preformed metal hydroxides to solution is the only way to ensure an adsorption mechanism is taking place, not co-precipitation. A review of the literature shows that magnesium and aluminum hydroxides are predominately being used for adsorption of monomeric silica (Iler, 1979; Salvador et al., 2013). This is most likely because silica adsorption by magnesium hydroxide is considered to occur during the common lime softening process, and aluminum hydroxide appears to have the most rapid silica adsorption kinetics of any metal hydroxide (Salvador et al., 2013). The downside of using these materials as adsorbents however is that they both have narrow pH ranges of insolubility. They both require large pH adjustments in solution to maintain insolubility driving up operation cost, especially in buffered water. Another issue is that if dissolved Mg^{2+} and Al^{3+} are liberated into solution, metal silicates will precipitate in subsequent processes (Salvador et al., 2013).

Ion Exchange

Ion exchange has been used for years providing thorough removal of dissolved silica in solution. The typical process consists of weak acid cation exchange for hardness removal, followed by strong base anion exchange for silica removal (Milne et al., 2014). The localized pH within the anion exchange resin is strong enough to de-protonate monomeric silica ($H_3SiO_4^-$) making it susceptible for exchange and removal from solution. For this reason, ion exchange is only effective for monomeric silica and cannot remove silica colloids. Many thermoelectric utilities worldwide utilize ion exchange for silica removal down to 0.03 ppm range (Iler, 1979). However, it is also common to have

precipitation and adsorption processes before ion exchange to preserve resin longevity and enhance removal (Iler, 1979).

Chemical Coagulation

Chemical coagulation implies the destabilization of stable silica particles in solution by compression of the electric double layer via salting out effects, charge neutralization, or inter particle bridging (Howe et al., 2012). Coagulation is most often executed by the addition of metal salts and long chain polymers to solution. Destabilized particles bridge together via Van Der Waals attraction and are removed from solution by flocculation and sedimentation (Howe et al., 2012). Metal salts and polymers have proven effective for destabilization of silica colloids but unfortunately have a low efficiency for dissolved silica removal (Milne et al., 2014). Huang and coworkers (2004) demonstrated effective coagulation of colloidal silica in IC wastewater using polyaluminum chloride (PACl) and polyacrylamide (PAA) in dead end micro filtration studies. Liu and coworkers (2012) showed 99% turbidity removal using $AlCl_3$ in synthesized IC wastewater containing silica colloids. $FeCl_3$ has not been rigorously evaluated for coagulation of silica colloids in both synthetic and real IC wastewater.

Electrocoagulation

Electrocoagulation is a newer technology that utilizes a sacrificial anode to remove silica from solution (Milne et al., 2014). The anode is typically aluminum or iron operated in the cathodic cycle liberating multivalent metal ions into solution. Metal cations neutralize surface charge of suspended particles, just as in chemical coagulation, allowing their removal through flocculation and sedimentation or membrane filtration.

Like chemical coagulation, electrocoagulation is most effective for the removal of silica colloids but may also remove dissolved monomeric silica. A study by Dan and Wang (2008) reported 80% removal of monomeric silica in brackish seawater by electrocoagulation. Electrocoagulation is a promising new method of silica removal however its feasibility in some applications may be hampered by two factors: First, to construct an electrocoagulation facility is a large initial investment some utilities may not be able to afford (Milne et al., 2014). Second, by using aluminum electrodes, often dissolved Al^{3+} is left in solution risking potential metal-silicate precipitation in subsequent processes (Milne et al., 2014).

Experimental Approach

This project evaluates the application of ferric chloride and ferric hydroxide in comprehensive removal of both silica colloids and dissolved silica from industrial wastewater to facilitate reuse. The first phase of this study was conducted at National Chiao Tung University (NCTU) in Hsinchu, Taiwan and evaluated silica colloid coagulation with ferric chloride in IC wastewater. The second phase of this study was conducted at the University of New Mexico (UNM), USA and evaluated monomeric silica adsorption with ferric hydroxide in RO process concentrate.

Justification for Ferric Chloride as Colloidal Silica Coagulant

IC manufacture is a predominant industry in Taiwan that has laid the groundwork for Taiwanese electronics manufacturing companies to flourish in markets around the world. Attributing to this, companies like TSMC, ACER, ASUS, MSI, and HTC are now names synonymous with innovation and quality. Hsinchu Taiwan, located on the upper west coast of the island, holds one of the largest hubs in the country for IC manufacture housed within the Hsinchu Technology Park. IC manufacture involves a process called photolithography that is used apply a thin film of photosensitive polymer to a silicon wafer. This thin film is exposed and developed to reveal a pattern on the wafer surface. Electro-metal deposition is used to create chip connections and features within this pattern. After deposition, a process called chemical mechanical planarization (CMP) is used to planarize, resurface and polish lithographic patterns, over-plated features, and oxide layers (Figure 10). CMP is similar to the common process of lapping, where an object becomes planarized and polished via the application of an abrasive compound on a rotary or vibratory surface. First phases of CMP require the use of diamond

slurries to remove large amounts of material at a fast rate. Final phases of CMP use colloidal silica for polishing and finishing. Colloidal silica slurry is rinsed from the wafer using UPW, which is generated on-site via RO for use throughout the entirety of the IC manufacturing process. The rinse stream, containing abundant colloidal silica slurry, is collected and pumped for on-site treatment. Colloidal nanoparticles must be removed before discharge of IC wastewater into domestic systems due to their role as a human and environmental hazard. Suspended silica particulate matter is susceptible for removal by coagulation by metal cations based on its negative zeta potential in solution (pH 10). Current literature has predominantly investigated removal of particulate silica matter with Alum, $AlCl_3$ and Poly aluminum chloride (Chuang et al., 2007; Liu et al., 2012). However, ferric chloride, another effective coagulant used in the water treatment industry, may be just as effective. Therefore, it is hypothesized that ferric chloride will be an effective and optimizable coagulant to remove particulate silica matter from IC manufacture wastewater generated in Hsinchu Taiwan.

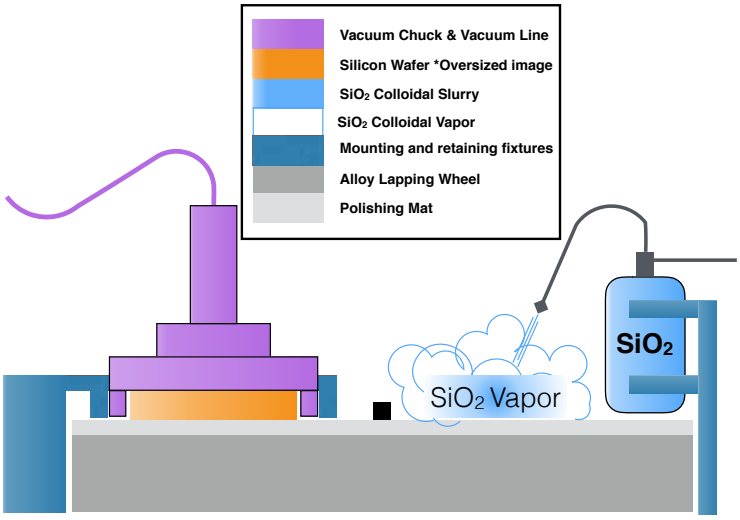

Figure 10. Typical chemical mechanical planarization setup used in IC manufacture

Justification for Ferric Hydroxide as Dissolved Silica Adsorbent

Motivation to use ferric hydroxide as a silica adsorbent was initiated by the Master's Thesis by Sims (2015). Sims (2015) used Ferric hydroxide as a supplemental material to facilitate silica removal with $Mg(OH)_2$; the combination provided enhanced removal compared to $Mg(OH)_2$ alone. Predominantly in literature, silica adsorption by hydrous iron oxides have aimed at understanding geochemical relationships between naturally occurring reactive silica and ferrihydrite. More recently authors have investigated silica removal with ferric hydroxide using synthetic waters. These investigations are based on equilibrium reactions and have not evaluated ferric hydroxide as a rapid silica removal agent to be applied industrially. Furthermore, application of ferric hydroxide in the removal of silica present in IC and RO wastewater has not been conducted to date. Therefore, there is a gap in the literature regarding a rigorous investigation of ferric hydroxide adsorption of silica present in these waste streams. This study will serve to fill this gap and establish the plausibility of using ferric hydroxide as an industrial silica adsorbent to facilitate water reuse. Further justification to use ferric hydroxide was based on a literature search revealing other facets of the material that may prove beneficial for rapid silica adsorption. The predominant factors for using ferric hydroxide are as follows:

4. Ferric hydroxide is capable of removing 99.8% of silica from solution in equilibrium experiments (McKeague, 1968)
5. Ferric hydroxide has rapid silica adsorption kinetics (Milne et al., 2014)
6. Ferric hydroxide has been proven effective in preliminary silica removal as pretreatment for ion exchange in boiler feed water (Iler, 1979)

7. Ferric hydroxide has a large range of insolubility and will likely not liberate metal ions into solution if pH varies, which is the case for $Al(OH)_3$ and $Mg(OH)_2$. Dissolved ions in solution run the risk of causing metal silicates to precipitate in subsequent processes (Salvador, et al., 2014).
8. Spent ferric hydroxide may be easier to dispose of than chemically complex precipitate sludges like those present in lime softening (Milne., 2014).

Based on this background investigation into the adsorption properties of ferric hydroxide, it was hypothesized that ferric hydroxide would be an effective agent for rapid silica removal in both IC and RO wastewater streams.

Materials

Integrated Circuit Wastewater

IC wastewater used in this study is typically pH 10, consists of UPW, contains high concentrations of both colloidal silica and reactive silica, and has trace amounts of metals, photosensitive polymers, and different oxides. The facility in Hsinchu Technology Park where the IC wastewater was produced utilizes a ceramic ultra-filtration membrane array to concentrate its waste stream and extract water for reuse before coagulation treatment. After being concentrated, the wastewater is fed to an on-site water treatment process involving pH adjustment, rapid mix, coagulation, flocculation and settling. The water treatment group at the IC manufacturer uses $Al_2(SO_4)_3$ as a colloidal silica coagulant, landfills settled silica matter and discharges supernatant to the sewer system. For this work, both pre-concentrate and post-concentrate streams were collected and transported back to NCTU for storage and analysis (Table 2).

Table 2. Characteristics of IC wastewater as sampled

CMP Wastewater	Pre Concentrate	Post Concentrate
pH	10.1	*9.67
Turbidity (NTU)	132	243
Conductivity ($\mu S/cm^2$)	86.3	136.6
Zeta Potential (mv)	-46.5	-41*
*Sample was stored for 2 days in atmospheric conditions before being tested and pH dropped		

Reverse Osmosis Concentrate

RO wastewater was generated on-site at UNM. The concentrate stream from a reverse osmosis system (GE Osmonics, USA) processing tap water at 75% recovery was used

in adsorption experiments. The GE system utilized 3 RO membranes in series and was operated to generate a concentrate stream near the solubility limit for reactive silica in solution (~120 mg/L). Table 3 shows the RO concentrate characteristics.

Table 3. RO Concentrate as samples from GE Osmonics system

pH		Silica Content (mg/L)		Conductivity (μS/cm^2)			
8.3		125		755			
ICP-OES				**Ion Chromatography**			
Element	mg/L	Element	mg/L	Element	mg/L	Element	mg/L
Ba^{+}	0.23	Na^{+}	83.88	F^{-}	1.60	NO_3^{-}	5.17
Ca^{2+}	89.77	Pb^{2+}	0.023	Cl^{-}	86.811	SO_4^{2-}	218.88
Cu^{2+}	0.02	SiO_2	125.4	**Carbonate**		**Charge Balance**	
K^{+}	13.86	Sr^{2+}	1.06	Species	mg/L	Error	
Li^{+}	0.24	As	0.032	CO_3^{2-}	24	2.28%	
Mg^{2+}	19.06			HCO_3^{2-}	140		

Chemical Coagulant

Industrial 45% ferric chloride (Jongmaw, Taiwan) was diluted to 0.062M as Fe^{3+} and used for coagulation dosing. pH adjustments were done with 0.33M NaOH solution made from 97% NaOH reagent pellets (Sigma Aldrich, USA) and 0.133M HCl solution made from 12M HCl solution (Sigma Aldrich, USA).

Chemical Adsorbent

Amorphous ferric hydroxide for adsorption experiments was precipitated in situ to eliminate the potential for lost material. 45% ferric chloride (Jongmaw, Taiwan, or Oakwood Chemical USA) was diluted to make a 1M Fe^{3+} stock solution. Fe^{3+} stock was administered into either a B-KER^2 rectangular batch testing jar (Phipps and Bird, USA) for sequencing batch reactor (SBR) studies or 500mL Nalgene bottles for equilibrium

studies. 2.5M NaOH made from 97% reagent pellets (Sigma Aldrich, USA) was added in a 3:1 molar ratio of OH^-/Fe^{3+} ratio to rapidly precipitate ferric hydroxide solids. DI water was added in 1L total volume for SBR studies and 400mL total volume for equilibrium studies to increase solution volume facilitating pH adjustments and also to act as a preliminary rinse for the precipitate. pH was adjusted to 7.5 using 0.33M NaOH and 0.13M HCl solutions. Ferric hydroxide solids were allowed to settle for one hour and the iron free supernatant was decanted and discarded. DI water was added once more as a secondary rinse, pH was once again adjusted to 7.5, the solids were settled for another hour and supernatant discarded. Only two rinses of the ferric hydroxide precipitant were executed as it may not be feasible to implement multiple rinses in actual industrial application.

Methods

Coagulation

Coagulation experiments were conducted using a PB-900 programmable Jar tester (Phipps and Bird, USA). The mixing program used for this study is reported in Table 4.

Table 4. Coagulation Mixing Procedure

Step	Pre Agitation	Rapid Mix	Flocculation	Settling
Program Assignment	MX1	MX2	MX3	MX4
RPM	200	300	30	0
Time (min)	1	1	20	30

Coagulation optimization experiments for pre-concentrate IC wastewater consisted of 2 steps, and coagulation optimization for post-concentrate water consisted of 3 steps. Post concentrate water was studied more heavily because it was the actual feed water for coagulation at the IC facility. Coagulation experiments proceeded initially with variable Fe^{3+} dose and no pH adjustment generating a curve ranging from negative to positive zeta potential along with high to low turbidity (Step #1). The optimal dose was determined to be at the location of zeta potential closest to zero and corresponding lowest turbidity. Optimal dose was then translated to a series of experiments with controlled pH during rapid mix to determine the optimal pH conditions for coagulation (Step #2). pH was controlled by initially dosing with acid or base during pre-agitation, and further pH adjustment was executed if necessary after the coagulant dose. All pH adjustments after coagulant dosing occurred within the rapid mix phase. For post concentrate water, once an optimal pH was determined, dosing amount was once again

varied for further refinement (Step #3). Figure 11 is a diagram of the coagulation process used at NCTU. Coagulant dose was consistently administered under the solution surface to simulate inline rapid mixing. Coagulation particle size was determined with a Nano Sizer (Malvern, UK) and aqueous phase images were taken with a FloCAM (Fluid Imaging Technologies, Inc., USA). Ferric hydroxide was also briefly evaluated for coagulation capacity using pre-concentrate water. The molar amount of ferric hydroxide used was based on the dose of ferric chloride effective for coagulation in pre-concentrate water. Ferric hydroxide showed no coagulation capacity and its use was discontinued.

Table 5. Coagulation Process

Coagulation Process						
	Section # 1		**Section #2**			**Section #3**
Water Type	**Pre-Concentrate**		**Post-Concentrate**			**Pre-Contentrate**
Chemical Used	$FeCl_3$		$FeCl_3$			Fe(OH)3
Step in Process	Step #1	Step #2	Step #1	Step #2	Step #3	Step#1
Procedure	Vary dose w/o pH adjustment	Hold at optimal dose & vary pH	Vary dose w/o pH adjustment	Hold at optimal dose & vary pH	Hold at optimal pH & Vary dose	Dose at pH 5, 3 and 2.4
Characteristics used to evaluate dosing	ζ (mV)	ζ (mV)	ζ (mV)	ζ (mV)	ζ (mV)	ζ (mV)
	Turbidity (NTU)	Turbidity (NTU)	Turbidity (NTU)	Turbidity (NTU)	Turbidity (NTU)	Turbidity (NTU)
Outcomes	Optimal Dose (OD)	Optimal pH at OD	Optimal Dose	Optimal pH at OD	Optimal Dose at Optimal pH (Fine)	No Coagulation capacity

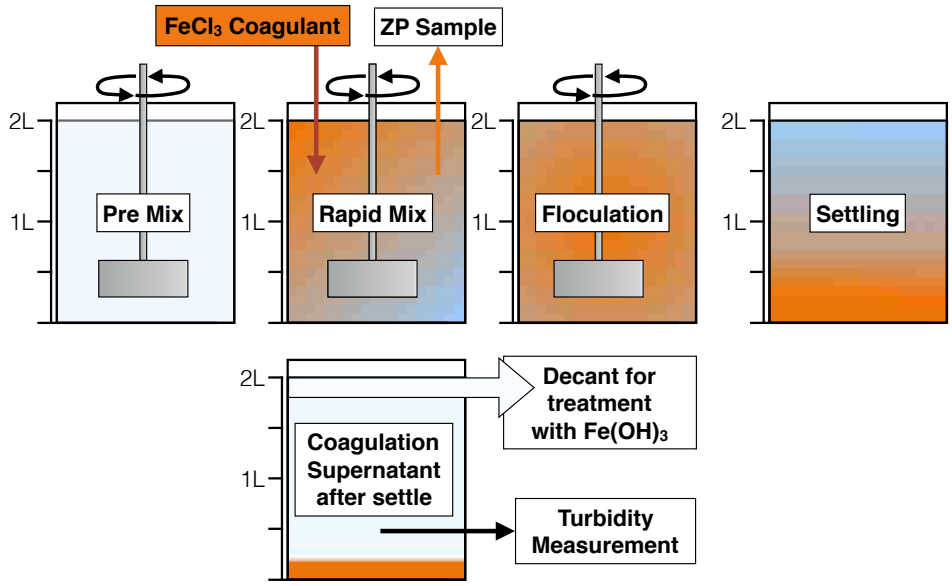

Figure 11. Coagulation process used for IC wastewater

Zeta Potential and Turbidity

All coagulation runs were evaluated by zeta potential measurement (Malvern, UK). After each rapid mix (MX2), a sample was taken and rapidly interrogated for zeta potential to determine coagulation effectiveness. Flocculant particle size was also determined using a NanoSizer (Malvern, UK) after each MX3 flocculation phase. Turbidity measurements were taken after each 30-minute settling phase (MX4) using a 2100P portable turbidimeter (HACH, USA). pH was monitored during all mixing phases with a SensION portable pH meter (HACH, USA). Conductivity was measured with a Clear CON200 (Oakton, USA).

Adsorption

Sequencing Batch Reactor

In the beginning phases of this work, equilibrium adsorption experiments were executed in order to get a better understanding for the silica adsorption capacity of amorphous ferric hydroxide in solution. After one such experiment had concluded, it was hypothesized that although ferric hydroxide had reached adsorption equilibrium with <100% silica removal, the material still had unused adsorption sites. In order to test this hypothesis, the adsorption supernatant was decanted off, re-filled with new silica containing water, and agitated on a shaker table at 100rpm for an additional 24 hours. This experiment exhibited continued silica removal from solution. This test was continued for 5 more iterations and silica was removed each time, although at decreasing removal percentages. The observations from this rough experiment were: 1) Amorphous ferric hydroxide adsorbent had increased silica adsorption capacity past what was observed with a single equilibrium experiment. 2) The total capacity of ferric hydroxide could be exploited by continually subjecting ferric hydroxide to water with the highest concentration of silica possible. The hypothesis generated from this experiment was that the maximum silica loading achievable on an adsorbent surface was more a function of silica concentration in solution than reaction time. If this hypothesis was correct, it would mean that maximum silica loading could be achieved with reaction times less than required for equilibrium as long as maximum silica concentration in solution was consistently maintained. In order to test this hypothesis experimentally, a sequencing batch reactor (SBR) approach was used. In these tests ferric hydroxide adsorbent was subjected to continual doses of wastewater, thereby maintaining a

maximum concentration gradient of adsorbate in solution to adsorbate on the adsorbent surface over time. Figure 12 is a diagram of the SBR process used.

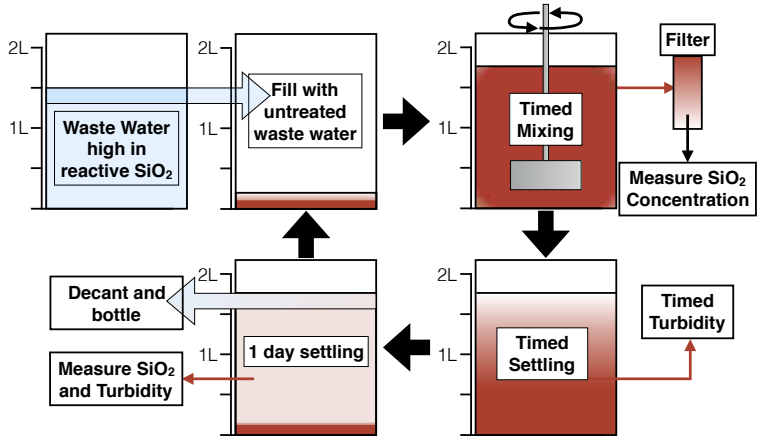

Figure 12. Operating scheme use for ferric hydroxide adsorbent

Adsorption of Silica in Coagulation Supernatant

$Fe(OH)_3$ was precipitated in situ at a ratio of 15.4 molFe/molSi based on a dose of 1.5L IC coagulant supernatant containing 118 mg/L SiO_2. Adsorption reactions were executed at pH 5 because this was the pH of the coagulated supernatant. After dosing the ferric hydroxide solids with supernatant water, the solution was stirred at 100 rpm for 30 minutes. 8mL samples were taken at 10, 15, 20, 25 and 30 minute marks during the reaction for kinetic analysis. Samples were syringe filtered through 0.2 μm membranes (Pall, USA), effectively stopping the adsorption reaction, and filtrate was collected in clean glass vials. 5mL of filtrate was pipetted (Eppendorf, Germany) and added to 5mL of DI water. This dilution was necessary because the HACH High Range Silica Method detection limit is 100 mg/L of silica and concentration of reactive silica in the CMP wastewater was above 100 mg/L. After mixing, the solution was left still for 24 hours in order to allow all the ferric hydroxide adsorbent to settle. The supernatant was

decanted and the adsorbent was dosed again. The experiment was iterated a total of 4 times.

Adsorption of Silica in RO Concentrate with SBR

$Fe(OH)_3$ was precipitated in situ at an intended ratio of 25 molFe:molSi based on a dose of 1.5 liters of RO concentrate water containing ~125 mg/L SiO_2. The dosing ratio for RO concentrate was higher than that of IC coagulation supernatant because of the anticipated complexity of the solution; silica was expected to have higher competition for adsorption in RO concentrate therefore requiring more adsorbent to achieve comparable removal. The solution was stirred at 100rpm for 60 minutes with 8mL kinetic samples taken at 5, 10, 15, 25, 35 and 60 minute marks. Samples were syringe filtered through 0.2 μm membranes (Pall, USA) and the filtrate was collected in glass vials. Once again, the filtrate was diluted by 50% in order to accommodate the testing range of the HACH High Range Silica Method. After the 60 minute adsorption time, solution was allowed to settle for 30 minutes and turbidity samples were taken at 5, 10, 15, 20, and 30 minutes. Settling samples were extracted with a 1-5 mL auto pipette (Cole Parmer, USA) at a constant beaker depth and tested on a 2100P portable turbidimeter (HACH, USA). The solution was once again allowed to settle for 24 hours and the supernatant was decanted, collected and refrigerated at 5°C. The adsorbent material was contained in the B-KER^2 vessel and was ready to receive another dose of RO concentrate. This experiment was iterated a total of 18 times.

Equilibrium Experiments

Equilibrium experiments were used as a metric to gauge and compare adsorption capacity of the SBR experiment. Equilibrium experiments proceeded with ferric hydroxide adsorbent being precipitated in situ at varying ratios using individual 500mL Nalgene bottles as reaction vessels. Ratios used for equilibrium experiments were 50, 10, 5, 3.33, 2.5, 2, 1.67, 1.33, 1.11, 0.66, 0.5, 0.4, 0.33, 0.29 molFe/molSi with RO concentrate containing ~125 mg/L of SiO_2. After solutions were prepared, they were adjusted to pH 7.75, sealed and laid horizontally on a shaker table. Solutions were shaken at 100rpm for 18 days. Samples were taken after the reaction period with a syringe and 0.2μm filter (Pall, USA). Silica concentration was analyzed via the High Range Silica Method (HACH, USA).

Equilibrium Multi-Dose

After completion of equilibrium adsorption experiments, supernatant from the reaction vessel containing an initial dose of 5 molFe/molSi was decanted. The residual solids were dosed again with RO wastewater and allowed to react for 1 week. This was continued for 4 iterations in order to achieve an understanding of silica-iron particle charge with time.

Adsorbent and Supernatant Characterization

After each adsorption run with RO concentrate, decanted supernatant was bottled and refrigerated at 5°C for later solute testing. Anion concentrations were determined using an ICS 1100 Ion Chromatography unit (Thermo Fisher, USA). Ion Chromatography leverages principals of ion exchange in order to isolate and quantify species within a sample solution. In this instance, a cation column was used which ionically binds

cations in solution allowing anions to elute. Ions leaving the column are detected and quantified via light absorbance. Cation concentration was evaluated with an Inductively Coupled Plasma with Optical Emission Spectroscopy (ICP-OES) unit (PerkinElmer, USA). ICP-OES uses a plasma generated by electromagnetic induction to break all molecules in a sample into atomic species. These liberated atoms then lose and regain electrons in the plasma environment which gives off signature light radiation. These emission frequencies identify which atoms are present in solution. Using a calibration curve, the intensity of light radiation given off by each species can be correlated to a solution concentration.

Adsorbent material was freeze dried with a FreeZone 4.5 system (Labconco, USA). Freeze dried adsorbent was characterized for atomic content using a Primus II ZXS X-ray Fluorescence Spectroscopy (XRF) unit (Rigaku, USA). XRF was used to determine the atomic ratios of silicon to iron in the adsorbent material. The technique subjects a hydraulically compressed sample to high energy X-rays which ejects inner shell electrons from atomic species within the sample. When electrons in the atom's outer orbitals fill these lower vacant energy states, they emit x-ray's with characteristic fluorescence. This fluorescence is used to determine the samples atomic composition. An X-ray Photoelectron Emission Spectroscopy (XPS) unit (Kratos, UK) was used to determine atomic oxidation states of atomic species in the adsorbent. XPS exploits the photoelectric effect of a material by bombarding a surface with x-ray's in order to generate electron ejection from different orbitals within an atom. By taking the difference in energy of the bombarding photons (hv), the kinetic energy of an emitted electron, and the work function of the material, electron binding energy can be deduced.

Higher binding energies are associated with inner shell orbitals, and lower binding energies are associated with outer shell orbitals. Knowing the binding energy of an electron provides insight into its oxidation state, and therefore the bonds the atom is involved in. Surface area was determined by physical adsorption with nitrogen gas following the Brunauer–Emmett–Teller method, or BET, with a Gemini 2360 BET Surface Area Analyzer (Micromeritics). BET analysis subjects an outgassed sample to a flow of N_2 gas under vacuum conditions. The N_2 physically adsorbs to the sample due to Van-Der Waals attraction, and is assumed to cover the entire surface conforming to a Langmuir isotherm. The difference in N_2 amount introduced to the outgassed sample, and N_2 that leaves the sample tube, is correlated to how much N_2 was adsorbed on the surface; providing surface area.

IC, ICP-OES, Alkalinity and XRF measurements were all conducted at the UNM Earth and Planetary Sciences Analytical and Geochemistry laboratory. XPS and BET were conducted at the UNM Center for Micro Engineered Materials laboratory.

Data Analysis

Mass Balance

In order to make sense of the sequencing batch reactor data, a mass balance was implemented. Complexity arises in that after each decanting, a small amount of residual water (50mL) with inherent silica content remains in the bottom of the jar. Therefore, the volume of this residual water, along with the amount of dosing water, were combined to determine the total amount of liquid in the system. From this approach, initial silica concentration in each run (C_i) would be a function of the concentration of silica in the dose (C_D), volume of the dose (V_D), the concentration of

silica in residual water (C_{RW}), the volume of residual water (V_{RW}) and the total liquid volume (V_L) defined as follows:

$$V_L = V_D + V_{RW} \quad (21)$$

$$C_i = \frac{C_D V_D + C_{RW} V_{RW}}{V_L} \quad (22)$$

After making this initial correlation, the concentration of each filtered sample (C_{f1},C_{f2}, C_{f3}, C_{f4}, C_{f5}, C_{f6}..C_{fK}), which segregates all solids via a 0.2μm filter, would be directly correctable to the initial concentration of each run (C_i).

Once initial concentration of silica in solution (C_i) and concentrations of silica with each sample (C_{fs}) were calculated, then the removal percentage with time (%R_k), amount of silica adsorbed between each sample in mols (A_K) and the sum of all silica adsorbed up-to time K in mols (A_{TK}) can be calculated.

$$\%R_K = \left(1 - \frac{C_{fK}}{C_{iK}}\right) \cdot 100 \quad (23)$$

$$A_K = \frac{\left(C_{fK-1} - C_{fK}\right)}{V_L} \quad (24)$$

$$A_{TK} = \sum_{K=1}^{n} A_K = \sum_{K=1}^{n} \frac{\left|C_{fK-1} - C_{fK}\right|}{V_L} \quad (25)$$

In order to accurately calculate the ratio of amount of silica (moles) adsorbed to the amount of adsorbent (moles) in the systems (silica loading), the amount of ferric hydroxide removed with each sample needed to be addressed. Each time a sample was taken 8mL of mixed solution was lost from the system; this occurred at a rate of 6 samples per run. The amount of ferric hydroxide remaining in solution after each

withdrawal (F_K) can be calculated knowing the amount of mols of ferric hydroxide existing in solution before the sample was taken (F_{K-1}), the total volume (V_T), which is a function of total liquid volume (V_L) and volume of adsorbent material (V_{ads}), and the volume of mixed solution removed by the syringe (V_S).

$$V_T = V_L + V_{ads} \quad (26)$$

$$Molarity_{Fe(OH)_3} = \frac{F_{K-1}}{V_T} \quad (27)$$

$$F_K = F_{K-1} - \left(\frac{F_{K-1}}{V_T} V_S \right) ; F_{K-1} > F_K \quad (28)$$

With ferric hydroxide loss accounted for, it is also necessary to account for the loss of adsorbed silica that was on the lost ferric hydroxide assuming homogenous adsorption. This can be calculated while calculating the molar ratio of silica adsorbed to mols of adsorbent (q_K) by taking the difference in adsorbent quantities and multiplying by the previous ratio of silica mols adsorbed per mol of ferric hydroxide, (q_{K-1}).

$$q_K = \frac{\left(A_{TK} - \left(F_{K-1} - F_K \right) q_{K-1} \right)}{F_K} ; q_K > q_{K-1} \quad (29)$$

Because q_K is inherently dependent on the amount of iron in the system, F_{k-1}, error arises if the volume of solution removed with each sampling is not consistent. In order to account for this, calculations for q_K were conducted taking into account a +/- 20% and +/- 15% change in iron assumed to be removed with each sampling to evaluate the sensitivity of the results to the sampling procedure.

Adsorption Modeling

A means to understand the interaction between an adsorbate and an adsorbing surface is by evaluating empirical adsorption results with either a Langmuir or Fruendlich isotherm model. Because experimental results exhibited a plateau in adsorption capacity, the Langmuir model provided the best fit for this work. The Langmuir isotherm derives from the assumption that all sites can bind only a single molecule of adsorbate, and all sites elicit the same change in energy with adsorption (Howe, et al., 2012). The Langmuir isotherm can be applied to empirical data by plotting the residual concentration of an adsorbate in solution [A] divided by the ratio of adsorbate to adsorbent (q_A) against the concentration of residual adsorbate in solution (Equation 30). This plot generates a series of points, that when fitted with a line, provides numerical values for $1/q_{max}$ and $1/K_{ads}[A]$. q_{max} being the adsorption capacity of an adsorbent when all sites are filled and K_{ads} the Langmuir adsorption constant. After finding q_{max} and K_{ads}, Equation 31 is used to determine the theoretical adsorption capacity (q_A):

$$\frac{[A]}{q_A} = \frac{[A]}{q_{\max}} + \frac{1}{q_{\max} K_{ads}} \quad \text{(30)} \quad \text{(Howe, et al., 2012)}$$

$$q_A = \frac{q_{\max} K_{ads} [A]}{1 + K_{ads}[A]} \quad \text{(31)} \quad \text{(Howe, et al., 2012)}$$

Surface Complexation Modelling

Typically, a more accurate way to model surface adsorption is by surface complexation analysis. Preliminary investigation into speciation of both the amorphous ferric hydroxide surface and silica in solution rendered an understanding of potential reactions to be include within the complexation model. Table 6 is an organization of expected

species in solution based on published formation constants. The speciation of the ferric hydroxide surface and silica in water are never opposite in charge; one is either neutral and the other charged, or both the same charge. This then indicates that what is considered “adsorption” is really an ionic bond between a silanol group and the iron surface.

Table 6. Speciation for ferric hydroxide and silica at various pH

Ferric Hydroxide and Silica Speciation								
pH	5	7	7.5		8	8.5	9	10
$Fe(OH)_3$ Surface		pK_{a1} 6.93[1]	pH_{ZPC} 7.85[2]			pK_{a2} 8.72[1]		
Major	$\equiv FeOH_2^+$	$\equiv FeOH_2^+$ $\equiv FeOH$	$\equiv FeOH$	$\equiv FeOH$	$\equiv FeOH$	$\equiv FeOH$ $\equiv FeO^-$	$\equiv FeO^-$	$\equiv FeO^-$
Minor	$\equiv FeOH$		$\equiv FeOH_2^+$	$\equiv FeOH^+$ $\equiv FeO^-$	$\equiv FeO^-$		$\equiv FeOH$	
Silica Monomer								pK_{a1} 9.81[3]
Major	H_4SiO_4							H_4SiO_4 $H_3SiO_4^-$
Minor						$H_3SiO_4^-$		
Silica Dimer				pKa_1 8.1[3]				
Major	$Si_2O(OH)_6$			$Si_2O(OH)_6$ $Si_2O_2(OH)_5^-$		$Si_2O_2(OH)_5^-$		
Minor	$Si_2O_2(OH)_5^-$				$Si_2O(OH)_6$			

Properties of Ferric hydroxide and monomeric silica in solution according to [1]Hansen et al., (1994), [2]Dzombak and Morel (1990), [3]Milne et al., (2014)

Modeling for this study stems from work done by Dzombak and Morel (1990) in their text “Complexation Modeling of Hydrous Ferric Oxide”. Hansen et al., (1994) applied the Dzombak and Morel (1990) complexation model to silica adsorption and developed

surface acidity constants of hydrous ferric hydroxide along with adsorption constants for the adsorption of silica onto hydrous ferric hydroxide.

(32) $\equiv FeOH_2^+ \leftrightarrow \equiv FeOH + H^+$ $pK_{a1} = 6.93 \pm 0.12$ (Hansen et al., 1994)

(33) $\equiv FeOH \leftrightarrow \equiv FeO^- + H^+$ $pK_{a2} = 8.72 \pm 0.17$ (Hansen et al., 1994)

(34) $\equiv FeOH + Si(OH)_4 \leftrightarrow \equiv FeOSi(OH)_3 + H_2O$ $pK_1 = -3.62$ (Hansen et al., 1994)

These equations, accounting for only monomeric silica adsorption, ultimately provided the best fit for the data generated by Hansen et al., (1994) at pH 3 and pH 5. However, Hansen and co-workers (1994) noted that about twice the amount of silica was adsorbed at pH 5 than pH 3, highlighting the trend of increased silica adsorption with increased solution pH with pinnacle near the pK_{a1} of silicic acid (Swedland et al., (2010), Dietzel, (2002)). In order to account for this trend, adsorption of dimers or surface polymerization are often accounted for in complexation models at pH above 5. Davis and coworkers (2002) found it necessary to incorporate adsorption of silica dimers to fit their experimentally produced data in the range of pH 5-9.5.

(35) $2Si(OH)_4 \leftrightarrow Si_2O_2(OH)_5^- + H^+ + H_2O$ $pK_a = 5$ (Davis et al., 2002)

(36) $\equiv FeOH + Si_2O_2(OH)_5^- + H^+ \leftrightarrow \equiv FeOSi_2O(OH)_4^- + H^+ + H_2O$ $pK_1 = -11.9$ (Davis et al., 2002)

(37) $\equiv FeOH + Si_2O_2(OH)_5^- \leftrightarrow \equiv FeOSi_2O(OH)_4^- + H_2O$ $pK_2 = -5.6$ (Davis et al., 2002)

Alternative to the concept of polymer adsorption or linear surface polymerization, Swedlund and co-workers (2010) used attenuated total reflectance with infrared spectroscopy (ATR-IR), to concluded that silica trimers are present on the hydrous iron surface. Their model accounts for two adsorbed silica tetrahedral monomers being bridged by a third. The surface complexation reactions they propose are as follows:

(38) $\equiv FeOH + H_4SiO4 \leftrightarrow \equiv FeOSi(OH)_3 + H_2O \quad pK_1 = -3.3$ (Swedlund et al., 2010)

(39) $\equiv FeOH + 3H_4SiO4 \leftrightarrow \equiv FeOH_2SiO_4^{-1} + H^+ + H_2O \quad pK_2 = 3.05$ (Swedlund et al., 2010)

(40) $2\equiv FeOH + 3H_4SiO4 \leftrightarrow Fe_2H_6Si_3O_{10} + 4H_2O \quad pK_3 = -15.33$ (Swedlund et al., 2010)

(41) $2\equiv FeOH + 3H_4SiO4 \leftrightarrow Fe_2H_4Si_3O_{10}^{-2} + 4H_2O + 2H^+ \quad pK_4 = -2.02$ (Swedlund et al., 2010)

Dietzel and coworkers (2002) on the other hand insist that no surface polymerization occurs above pH 6 for silica adsorption onto ferrihydrite. Their explanation is that if dimers, trimers, or oligomers adsorb to the hydrous ferric hydroxide surface, they quickly depolymerize leaving only monomeric silica. Taking all these reported results into account, surface complexation modeling was conducted with published adsorption constants, surface areas, and reaction stoichiometry to see what generated the best fit to experimental data.

Regeneration

Regeneration of ferric hydroxide as a silica sorbent goes hand and hand with increasing economic feasibility. As discussed by other authors, regeneration of iron adsorbent is considered difficult due to the robust coverage of silica on the hydroxide surface and the

strong covalent bond made between silicon and oxygen (Milne et al., 2014). However, most perspectives for metal hydroxide adsorbent regeneration attempt to find ways to remove silica while preserving the hydroxide material. Uniquely proposed and investigated in this work is the opposite approach: removing iron from the sorbed silica. This was achieved by solubilizing iron from ferric hydroxide and electro-depositing it onto a cathode via the application of an electrical potential in solution. This approach subsequently leaves highly concentrated silica in solution and removes iron from solution as a solid metal.

Solution Preparation and Electrochemical Cell

Soluble iron was generated from $\equiv FeOSi(OH)_3$. The electrochemical cell used in this work consisted of a 100mL glass jar with lid perforations to accept a working electrode, reference electrode, anode and nitrogen gas flow. The working electrode consisted of a carbon doped titanium mesh made in house. The reference electrode used was a Ag/AgCl sealed polymer. The anode consisted of a spiral wound titanium wire. Nitrogen gas was bubbled through solution to create an oxygen free environment. A preliminary CV scan was conducted in order to determine occurrence of a reduction peak. Deposition utilized the potential for reduction determined in the CV scan and occurred over 24 hours.

Results

IC Wastewater Characteristics

IC wastewater exhibited a large negative zeta potential, less than -40mV, at its native pH10 (Figure 13). Decreasing solution pH decreased particle repulsion in solution eventually resulting in a particle surface charge of -0.83mV at pH 2. This aligns well with published values of silica pH_{ZPC} of 2 (Iler, 1979). Colloid particle size increased slightly from ~137nm to ~152nm with pH decreasing from 4 to 1.5 where surface charge was between -20mV to 0mV (Figure 13) which fits the description of silica colloid behavior in solution by Iler (1979).

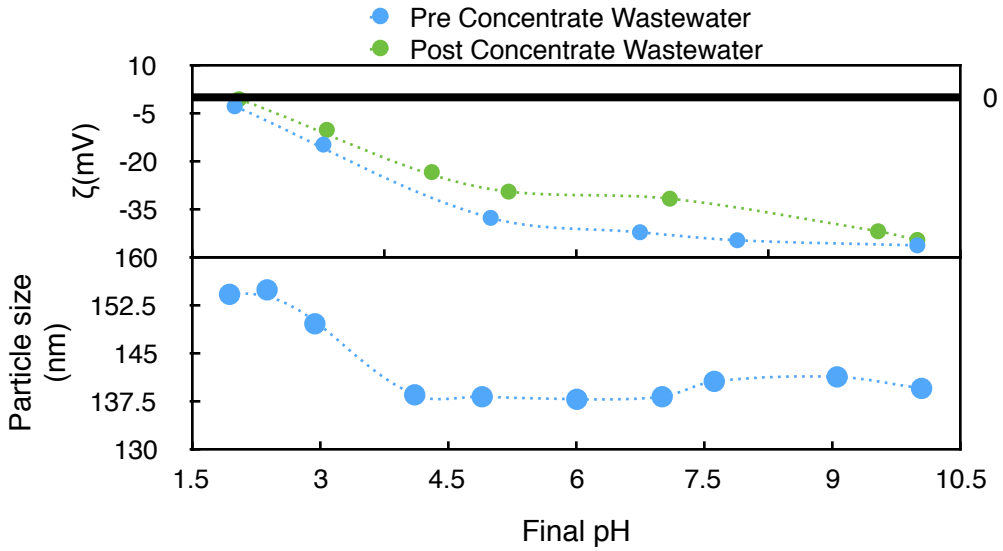

Figure 13. Surface charge and particle size of colloidal silica particles in pre and post concentrate IC wastewater

Coagulation: Pre-Concentrate

Initial dosing of 0.2 mmol/L as Fe^{3+} resulted in pH 7 and was not adequate to neutralize SiO_2 particles in solution exhibited by a strong negative zeta potential (-36.9mV) and high turbidity (Figure 14). Increasing dose to 0.24 mmol/L resulted in pH 5.6

corresponding to a zeta potential of -15.2mV and 27.9NTU turbidity (Figure 14). Further increasing coagulant dose to 0.25 mmol/L re-stabilized particles in solution to the positive regime and resulted in a zeta potential of 15.8mV and turbidity of 37.8NTU. Because a near zero zeta potential lied somewhere between 0.24 mmol/L and 0.25 mmol/L, it was deemed unreasonable to attempt dosing in increments between the two values. The conservative option of 0.24 mmol/L was chosen as an effective coagulation dose. Maintaining dose at 0.24 mmol/L and varying pH resulted in an optimal pH of 5 based on a zeta potential of -2.27 mV and turbidity of 6.1 NTU (Figure 15).

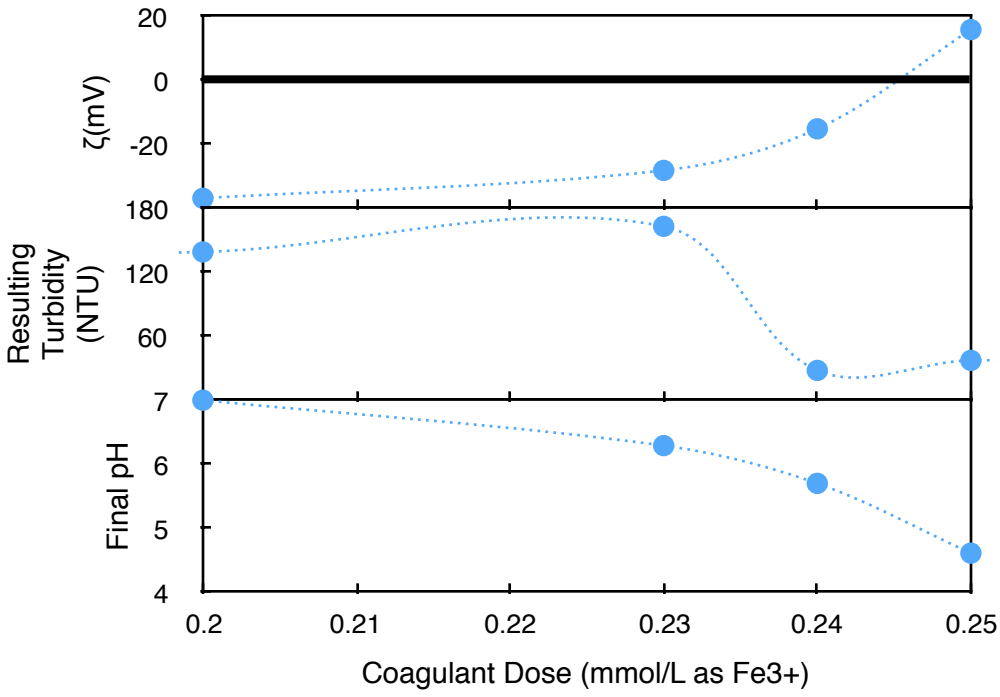

Figure 14. Final ZP, Turbidity, and pH after rapid mix with varying coagulant dose

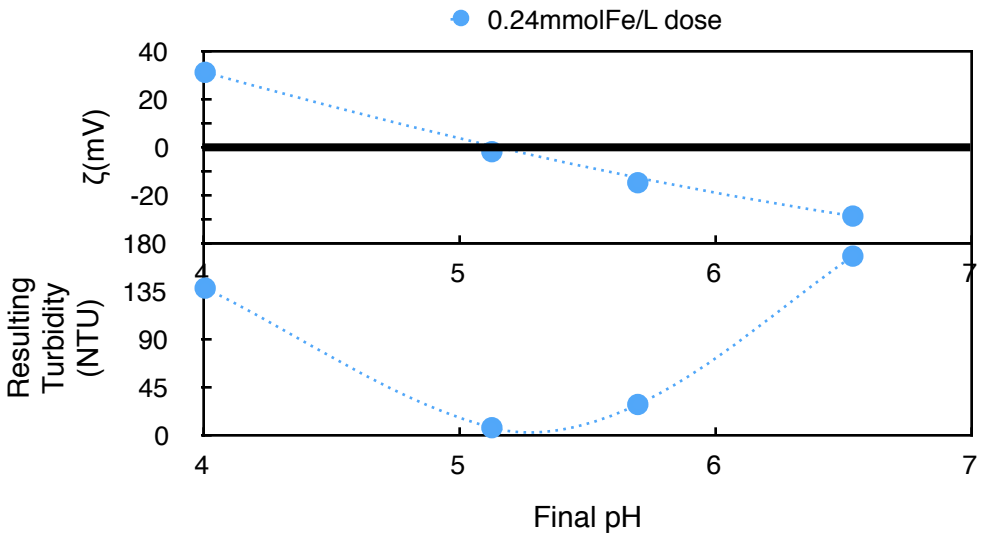

Figure 15. Resulting ZP and Turbidity after rapid mix with varying solution pH

Coagulation: Post-Concentrate

Post concentrate water required a higher dosing of coagulant compared to that of the pre-concentrate water due to higher turbidity and concentration of silica particles. Dosing from 0.25 mmol/L to 0.5 mmol/L resulted in a range of zeta potential values from -31.2 mV to 29.7 mV (Figure 16). The dose of 0.38 mmol/L was chosen to be effective corresponding to a zeta potential of -5.94 mV (Figure 16). Maintaining a dose of 0.38 mmol/L, pH was varied from 3.5 to 6. pH 5 resulted in a zeta potential closest to zero (-1.25mV) and a turbidity of 9.11 NTU (Figure 17). pH 4.75 resulted in the lowest turbidity of 7.63NTU and a positive zeta potential of +3.86 mV (Figure 17). PH 5 was chosen for use in further experimentation because it was an easily identifiable number. Maintaining pH 5 and varying Fe^{3+} dose from 0.3 mmol/L to 0.8 mmol/L produced zeta potentials in the range of -5 mV <ζ< 5 mV and turbidity below 10 NTU (Figure 18). Floc sized increased with increasing dose from 4-25 μm.

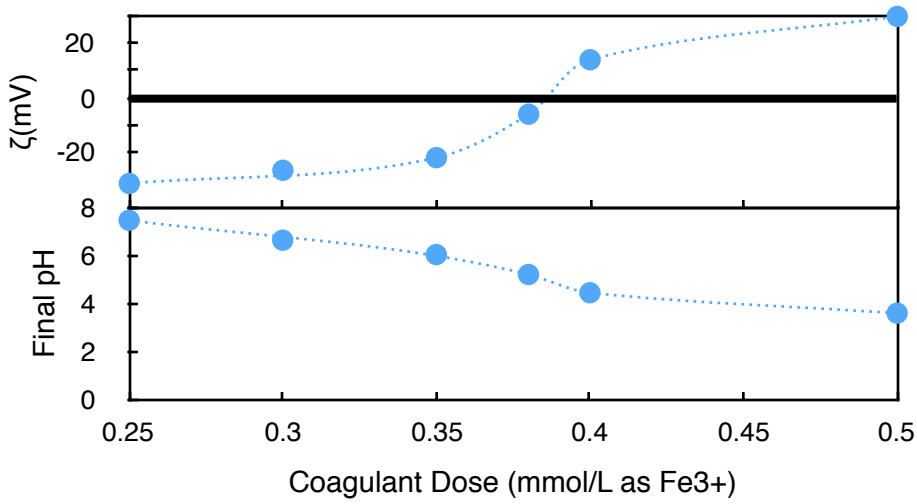

Figure 16. Resulting Zeta Potential and pH after rapid mix with varying coagulant dose.

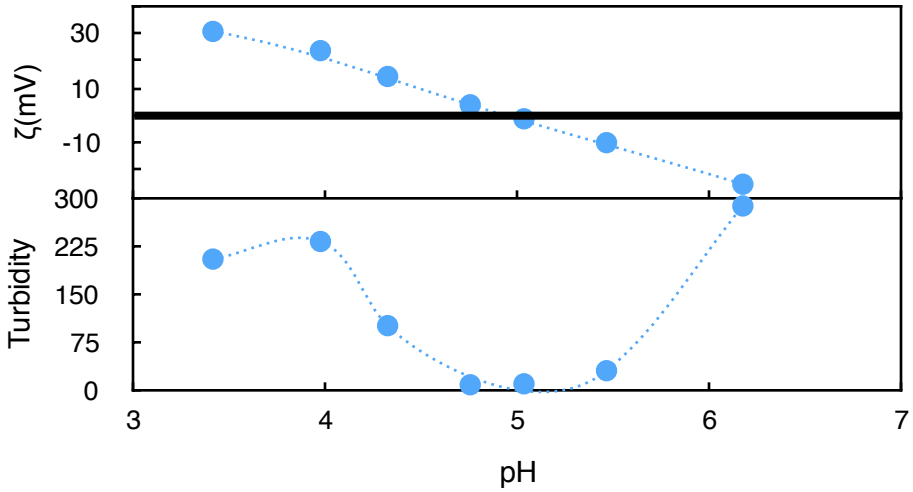

Figure 17. Resulting ZP (a) and Turbidity (b) after rapid mix with varying pH

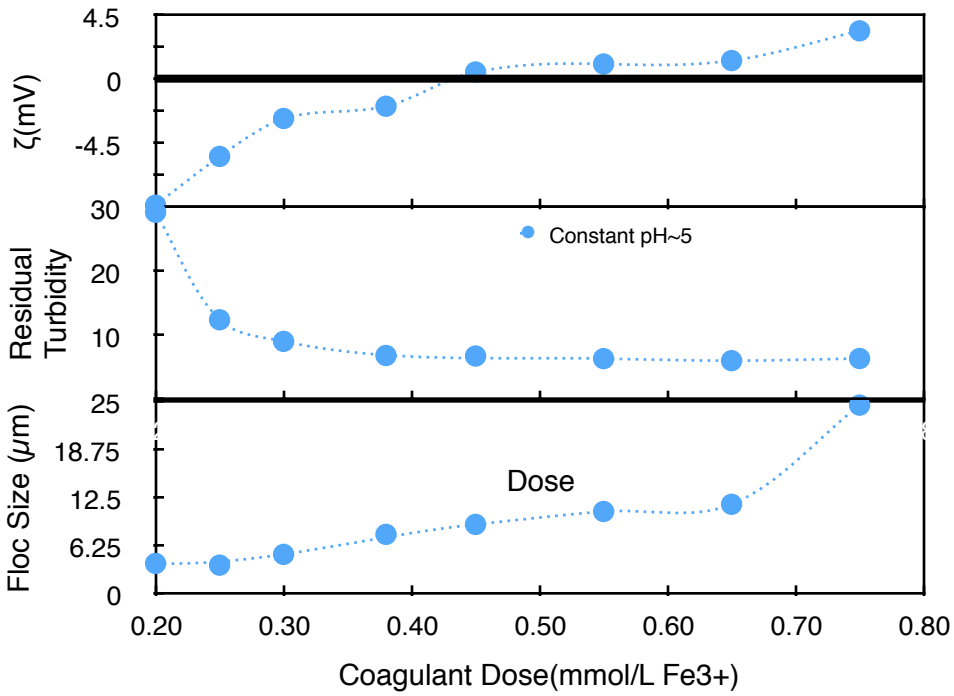

Figure 18. Resulting ZP (a), Turbidity (b), and Floc Size (c) after rapid mix with constant pH (5) and variable coagulant dose

Coagulation with Ferric Hydroxide

The surface charge of ferric hydroxide is contrary to surface charged observed by silica colloids in IC wastewater between pH 2 and 7.5 (Figure 19). Based on these findings, coagulation capacity of ferric hydroxide was evaluated at acidic pH's of 2, 3 and 5, where SiO_2 surface charge was at a minimum, theoretically enhancing the chances of surface neutralization by ferric hydroxide particles. However, no decrease in turbidity was observed at these pH's despite having near negative zeta potential for particles in solution (Figure 20). These results indicate that particle adsorption between silica colloids and precipitated ferric hydroxide is not a mechanism to achieve coagulation. Therefore, dissolved ferric ions in solution are necessary to destabilize silica colloids by charge neutralization.

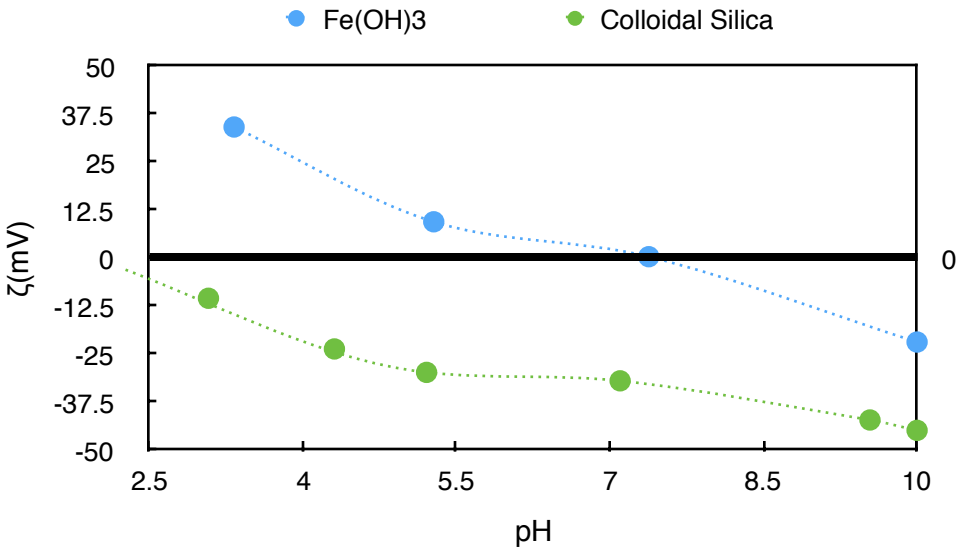

Figure 19. Comparison of surface charge between ferric hydroxide and colloidal silica at varying pH

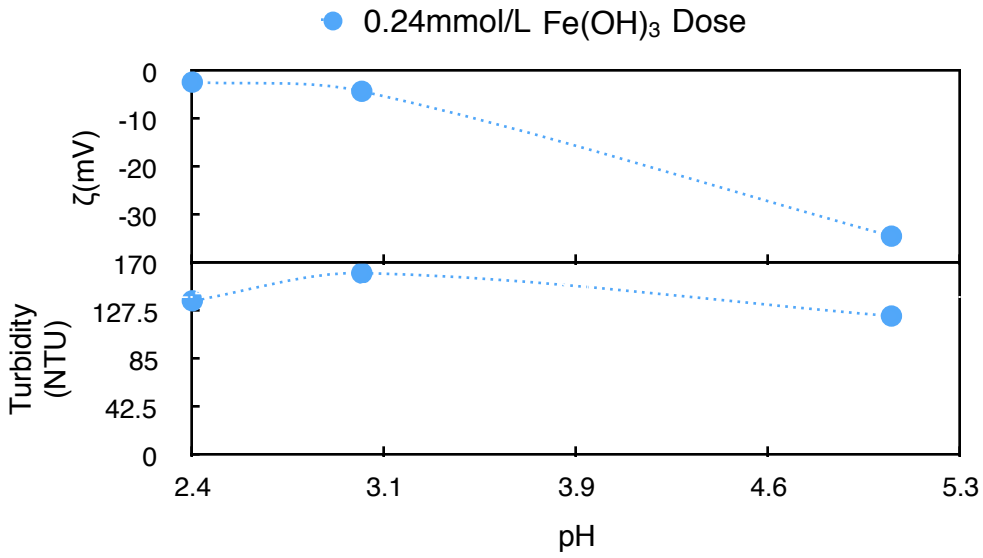

Figure 20. Final zeta potential and turbidity dosing IC wastewater with ferric hydroxide at different pH

SBR Adsorption

Adsorption of IC Supernatant

Treatment of CMP wastewater coagulation supernatant (118mg/L SiO_2) with ferric hydroxide at a dose of 15.4 molFe/molSi resulted in 92% removal of reactive silica from solution in 30 minutes (Figure 21). Subsequent runs, continuing the use of the same adsorbent material, resulted in 61%, 40% and 32% removal, respectively. Interestingly, although a total reaction time of 30 minutes was allowed, the data suggests that after 15 minutes removal rate begins to plateau in each of the 4 SBR runs. These results indicate that coagulation supernatant can effectively and rapidly be treated with ferric hydroxide to remove reactive silica in solution, making it viable for reuse as cooling water or potentially UPW production.

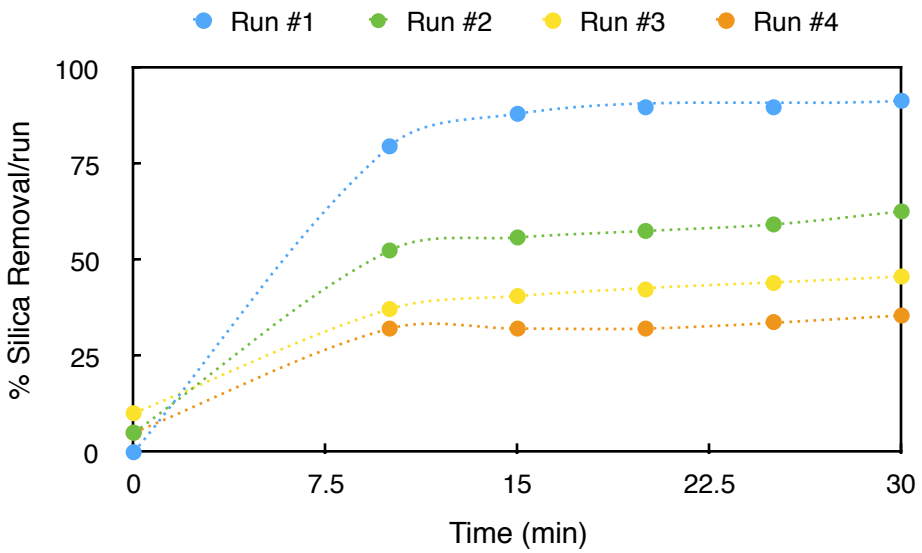

Figure 21. % Removal of reactive silica in multiple doses of IC wastewater using a single dose of ferric hydroxide at 15.4 molFe/molFe

Adsorption of RO Concentrate

Sequencing batch reactor experiments with 25 molFe/molSi using RO concentrate achieved 90% removal of reactive silica in 25 minutes and 94.57% removal

in 60-minutes for the first adsorption cycle (Figure 22). Subsequent runs continued to achieve reactive silica removal however with slightly decreased removal capacity each time. With 60-minute reaction time, greater than 50% silica removal was achieved with the 5th run, and greater than 25% removal was achieved with the 10th run. After 18 runs, silica removal was negligible (5%<) and the experiment was ceased. Isolated adsorption runs each have their own respective %Removal, however of real interest is cumulative silica removal. Cumulative silica removal would be the % Total Removal summing each isolated % Removal together. This is calculated by accounting for the total amount of water treated, and the total amount of silica removed. For instance, Run #3 achieved an isolated 74.7% silica removal, but when combined with the previous runs before it, Run# 1, 2 and 3, the total silica removal is 84.1%. Cumulative silica removal is reported in Figure 25 and compared with removal in equilibrium experiments. These results further elaborate on trends found in IC silica adsorption, and establish the case that using multiple adsorption cycles on a single adsorbent dose will serve to fully utilize the materials capacity. This implies that an effective reactor design would have multiple reactors in series, each with isolated adsorbent material. As the first reactor's adsorption capacity is expired, the remaining reactors would compensate and remove silica in accordance to process requirements. This would continue until the first reactor's adsorption capacity was completely spent, indicating complete utilization of the

ferric hydroxide. The first reactor's adsorbent could then be recharged, and set as last in the sequence.

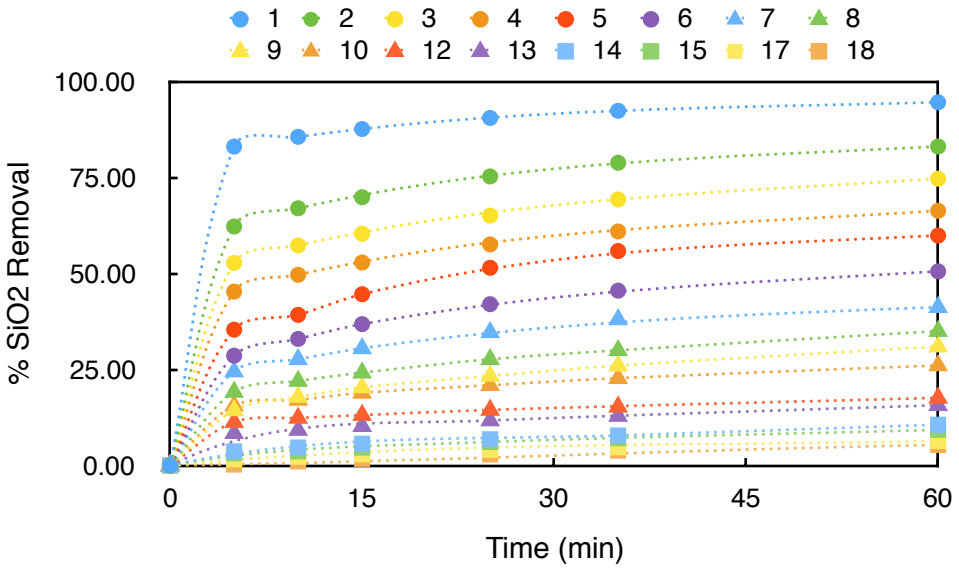

Figure 22. % Removal of reactive silica in multiple doses of RO-concentrate using a single dose of ferric hydroxide at 25 molFe/molSi

Turbidity

Solution turbidity during mixing exceeded the 2100P's detection limit. 30-minute solution settling after each adsorption run resulted in turbidity below 60NTU from for the first 5 runs, followed by an increase to 108 NTU after 6 runs, then a stark increase to a maximum of 627 NTU after 10 runs (Figure 23). Subsequent runs exhibited a trend of decreasing turbidity eventually reaching 232 NTU on the 18th run. Turbidity from a secondary blank reactor that was ran in parallel to the SBR reactor maintained a constant 30 minute turbidity below 20 NTU. This data shows that increased turbidity is directly correlated to increased silica adsorption. Conversely, less silica adsorption results in increased settling rate. These results indicate a means to segregate spent ferric hydroxide particles in reactor applications. Particles with low loading settle rapidly and can likely be retained with implementation of a settling basin. Particles with high

loading remain suspended in solution and do not settle out (due to increased particle repulsion (Figure 26), meaning they are likely candidates for removal by chemical coagulation.

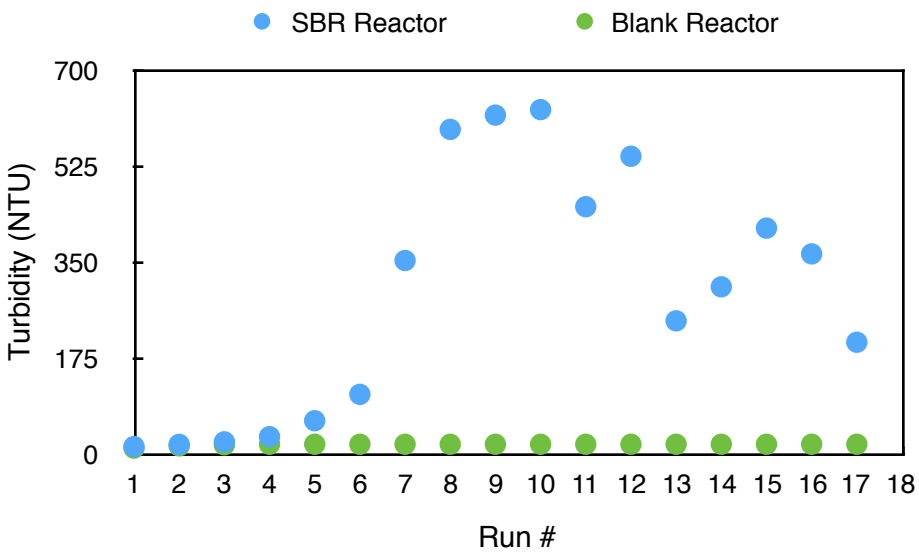

Figure 23. Turbidity after each adsorption experiment

Equilibrium adsorption

18-day equilibrium adsorption experiments with RO concentrate and varying amounts of ferric hydroxide adsorbent generated an adsorption isotherm for this system (Figure 24). The highest dose, 50 molFe/molSi resulted in 99% removal of reactive silica in solution, and a trend of decreasing removal with decreasing ferric hydroxide dose was observed thereafter. Equilibrium experiments were used to compare with SBR silica removal capacity and also for adsorption modeling. Comparatively, equilibrium experiments resulted in greater silica removal at relative dosing ratios than sequencing batch reactor experiments (Figure 25). This was to be expected as equilibrium reaction vessels had 18 days to react, and SBR experiments only had 1 hour reaction time per run. However,

it is interesting to note that the sequencing batch reactor experiments achieved comparable removal to equilibrium experiments.

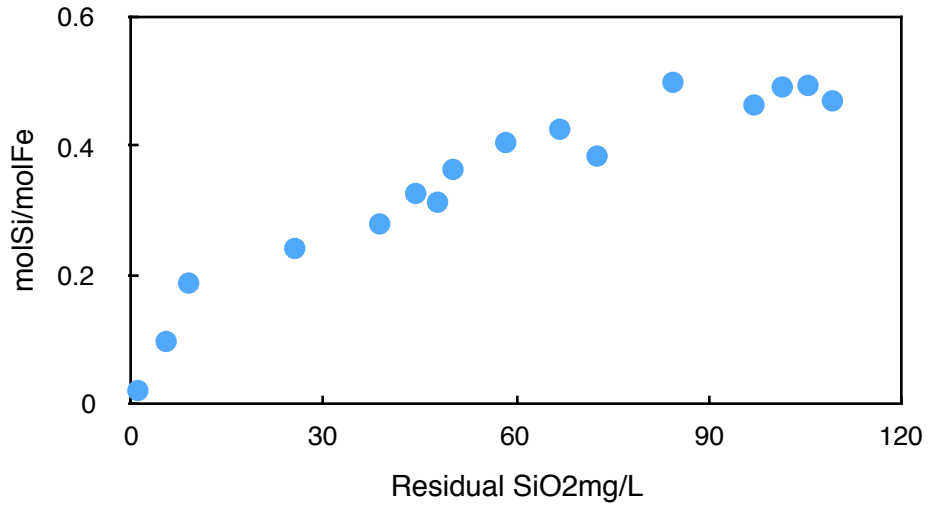

Figure 24. Adsorption isotherm of reactive silica adsorption in RO concentrate with 18-day reaction time

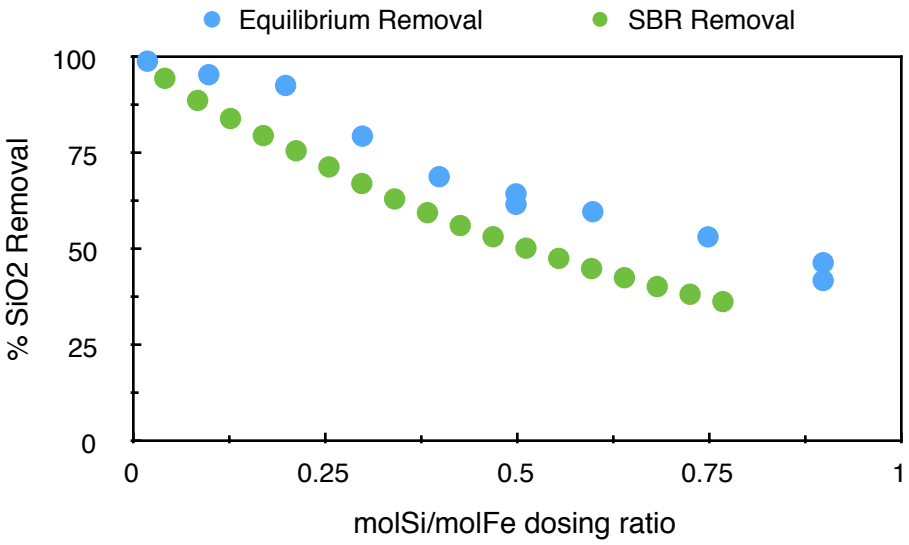

Figure 25. Percent Silica removal in SBR compared with equilibrium

Equilibrium Multi-Dose Experiments

Equilibrium multi-dose experiments resulted in continued removal for 4 iterations. With each new dose corresponding to additional silica removal from solution, the loading of silica onto the ferric hydroxide surface also increased. Consequently, particle zeta potential increased in magnitude (Figure 26) with each adsorption run. This study was conducted to test the hypothesis that the reason for decreased settling in SBR experiments was because of increased silica adsorption. This hypothesis was validated as it was shown that with increased silica loading, there was increased particle repulsion, which would lead to decreased settling. This data shows that ferric hydroxide particles loaded with silica are stabilized in solution and susceptible to coagulation techniques.

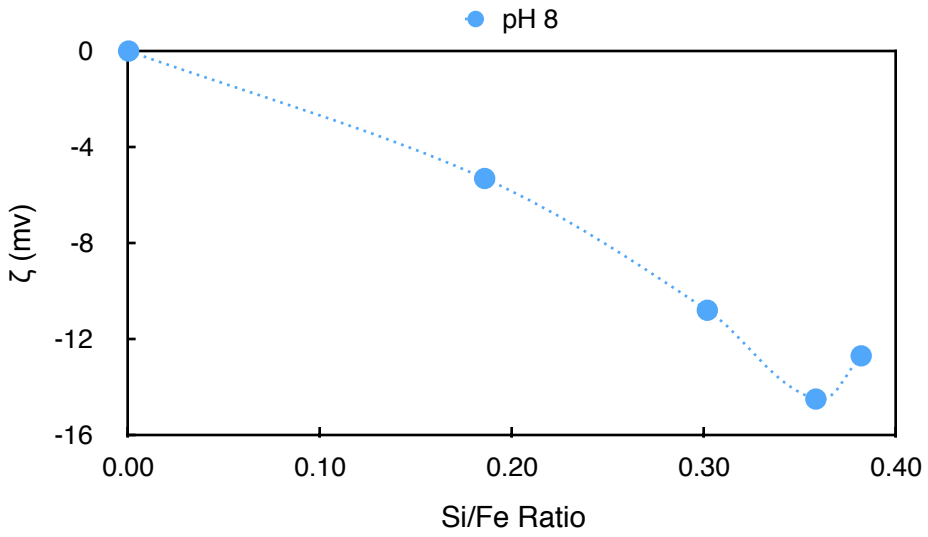

Figure 26. Increasing negative surface charge with increased silica loading

ICP-OES Results

ICP-OES results from SBR and equilibrium experiments show interaction between various cationic constituents and the hydrous ferric oxide surface. For discussion, the

cations are divided into three groups base on concentration in adsorption supernatant, which are dependent on initial concentrations of each constituent in the RO concentrate water used. The constituents above 5 mg/L residual concentration include calcium, potassium, magnesium, sodium and silica. Constituents less than 5 mg/L but above 0.25 mg/L residual concentration include lithium and strontium. Constituents below 0.25 mg/L include arsenic, barium, iron and lead.

Cation Concentration Greater Than 5 mg/L

For SBR experiments, calcium concentration is completely depleted from solution with the first adsorption run, then returns to initial concentration after 3 adsorption cycles (Figure 27). This is explained by observations made by Dzombak and Morel (1990) that state ferric hydroxide has strong calcium-specific adsorption sites. After 5 adsorption cycles, calcium concentration begins to continuously decrease from solution until completion of the experiment. This may be explained by continued selective calcium adsorption as the ferric hydroxide surface is subjected to continual doses of RO concentrate, forcing other species to desorb. Or, most likely, may be attributed to formation of calcium carbonate precipitates in the RO concentrate sample used for dosing which was continually exposed to the atmosphere. For equilibrium adsorption experiments, the largest calcium removal was observed with the largest doses of ferric hydroxide (Figure 28). Sodium concentration for SBR experiments is seen to be slightly lower than initial concentration with the first run, indicating slight absorption of sodium with ferric hydroxide (Figure 27). By the third run, sodium concentration reaches a maximum in solution, perhaps due to desorption of previously adsorbed sodium, or analytical variance. Sodium concentration in equilibrium experiments (Figure 28)

fluctuate sporadically because thoroughness of DI washing varied slightly with each container. Potassium and magnesium in Figures (26) and (27) both show initial removal and with subsequent samples return to initial RO water concentrations. For SBR experiments silica is observed to slowly increase in solution concentration with number of runs indicating a decrease in silica adsorption capacity of the ferric hydroxide surface. For equilibrium experiments, silica is observed to increase in solution concentration with decreasing ferric hydroxide dosing.

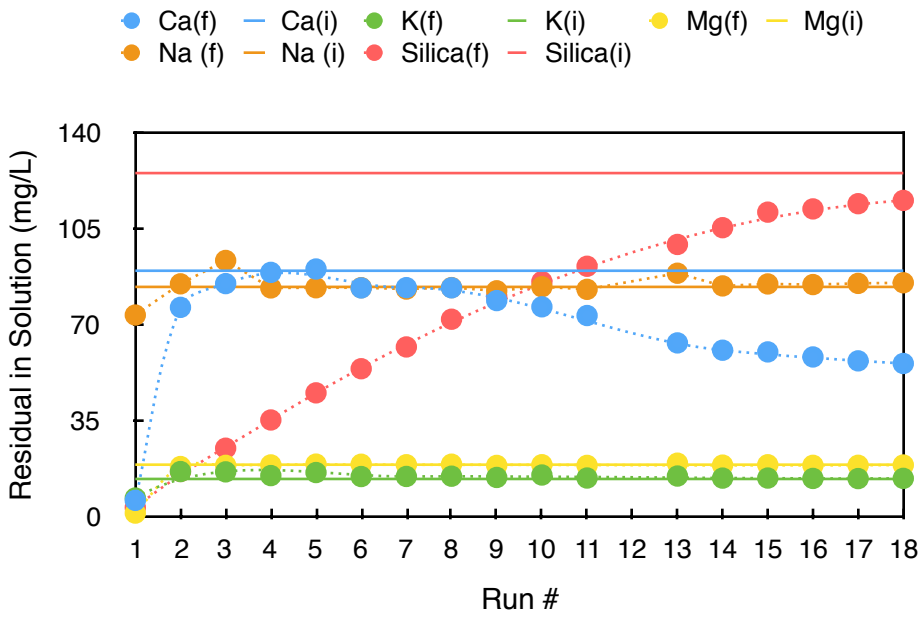

Figure 27. Major cation and silica concentration as determined by ICP-OES for each adsorption cycle

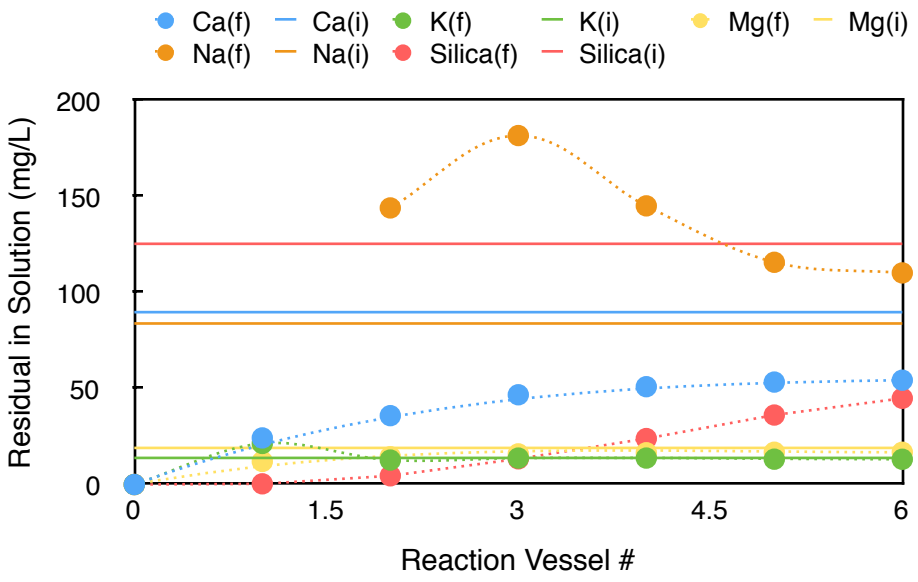

Figure 28. Major cation and silica concentration as determined by ICP-OES for each adsorption cycle

Cation Concentration Less Than 5 mg/L but Greater Than 0.25 mg/L

Lithium exhibited adsorption to the iron surface for both the first SBR run and the first equilibrium reaction vessel which had the highest dose of ferric hydroxide. Subsequent SBR runs exhibited expired lithium adsorption capacity (Figure 29). Equilibrium reaction vessels with adsorbent concentration less than the first reaction vessel do not exhibit lithium removal (Figure 30). Strontium however, had continued removal from solution for both SBR experiments and equilibrium studies. After 18 SBR adsorption cycles strontium never returned to initial solution concentration. This implies that hydrous ferric hydroxide may have specific adsorption capacity for strontium, while also accommodating adsorption of other cations. Equilibrium studies mirror adsorption of strontium in SBR experiments and exhibit adsorption capacity relative to abundance of ferric hydroxide dose.

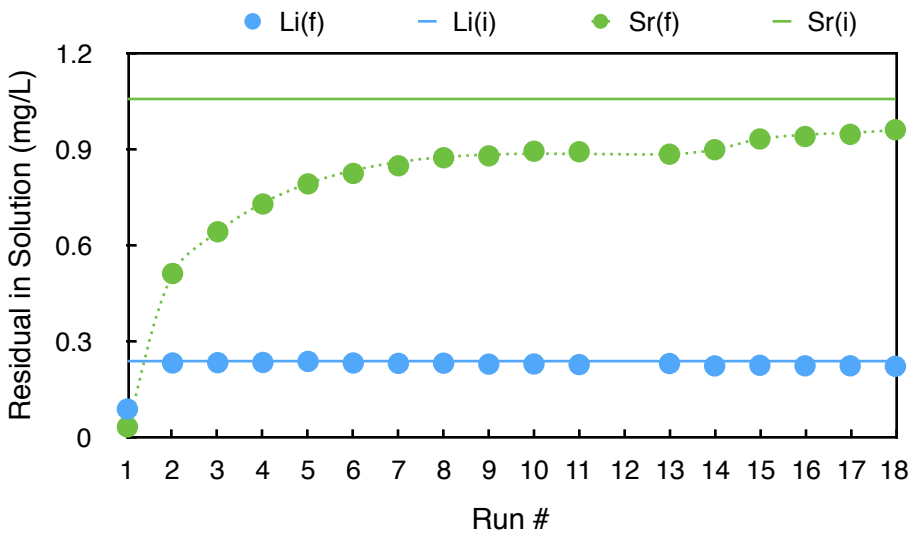

Figure 29. Minor cation concentration below 1mg/l as determined by ICP-OES for each SBR adsorption cycle

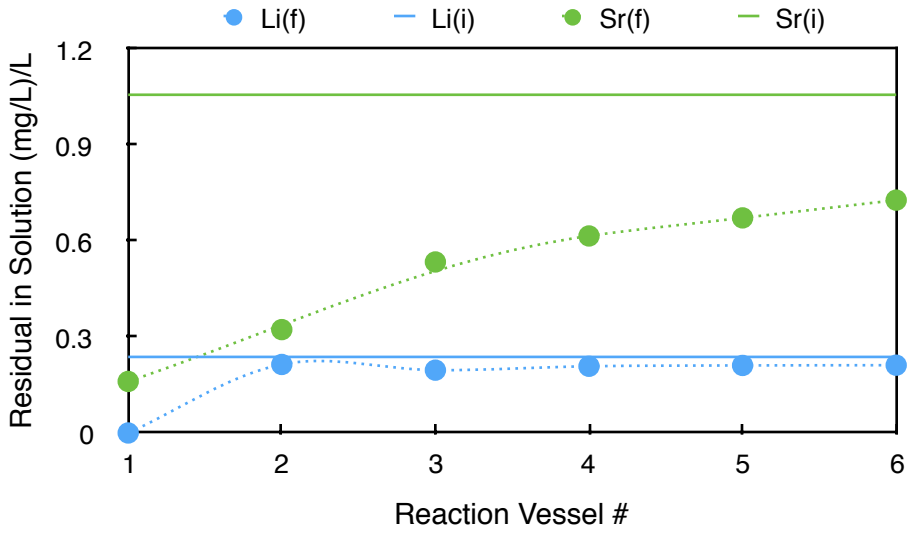

Figure 30. Minor cation concentration bellow 1 mg/Las determined by ICP-OES for each equilibrium adsorption vessel

Cation Concentration Less Than 0.25 mg/L

For SBR experiments there is removal of arsenic from solution with the first run, followed by an increase in solution concentration greater than initial, then maintained continual concentration below initial concentration (Figure 31 & 32). In SBR experiments, Barium shows an interesting trend with concentrations continually lower

than initial amount, then finally exceeding initial concentrations with dose #15 (Figure 31). For equilibrium experiments, Barium removal was consistent through all experiments and never returned to initial concentration (Figure 32). In SBR, Lead adsorption is evident with the first adsorption run thereafter returning to initial concentration (Figure 31). Equilibrium studies showed minimal but continual removal of Lead in all samples (Figure 32). Iron was not present in the RO concentrate used, so any amount detected in the adsorption supernatant would have come from dissolution of the adsorbent. Iron concentration showed up in SBR experiments for run numbers 9, 10, 11, 13, 14, 15, and 16 but all below 0.2 mg/L. All other runs had a negative value for iron concentration. With this sporadic fluctuation of iron concentration, especially at such low concentrations, it is concluded that any iron concentration in the supernatant cannot be determined with confidence and assumed zero. Equilibrium studies show a trend of increasing Fe^{3+} in solution with decreasing adsorbent dose (Figure 32). This likely due to the fact that solubility in solution is a function of concentration, making lesser doses more susceptible to dissolution.

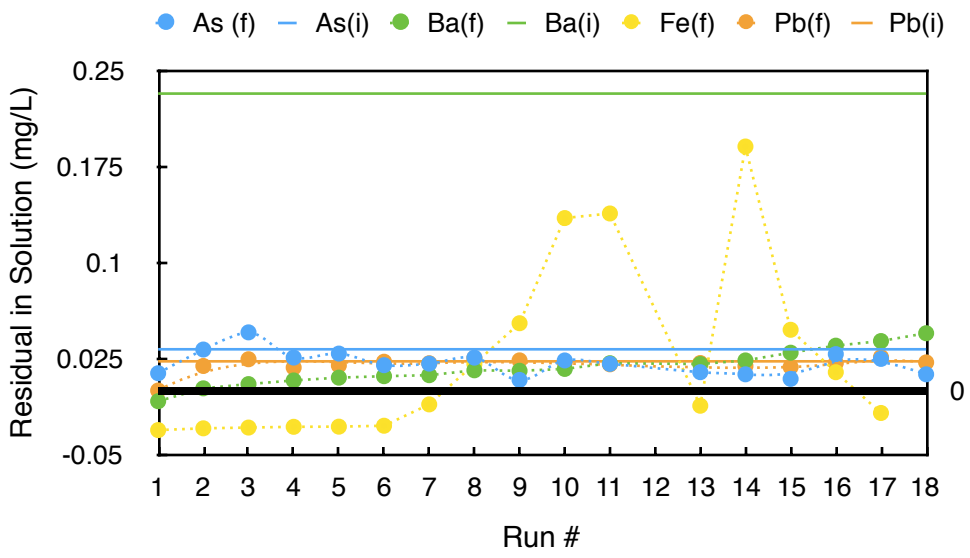

Figure 31. Minor cation concentration as determined by ICP-OES for each adsorption cycle below 0.5 mg/L

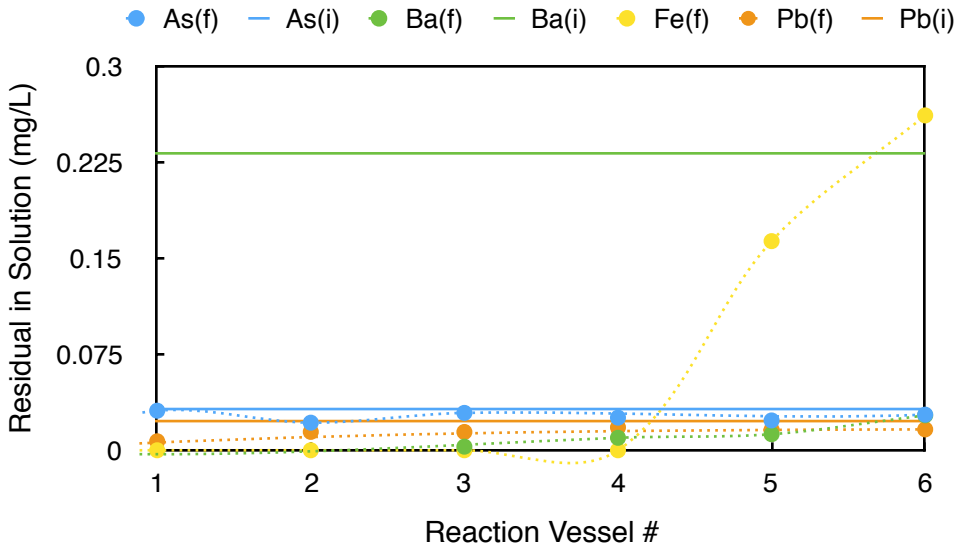

Figure 32. Minor cation concentration in equilibrium adsorption supernatant

Ion Chromatography

IC results exhibit the interaction between anions in solution and the ferric hydroxide surface during adsorption. For SBR experiments, chloride is seen to start slightly higher than equilibrium concentration and return to initial solution concentration within 4 runs

(Figure 33). Higher than expected chloride concentrations in SBR can be attributed to residual chlorine from the initial reaction of ferric chloride and sodium hydroxide to precipitate ferric hydroxide; which eventually gets rinsed away with continual runs. Chloride concentrations fluctuate in equilibrium tests because rinsing between each reaction vessel may not have been entirely consistent (Figure 34). Fluoride and Nitrate show little change in initial concentration when subjected to hydrous ferric hydroxide in SBR (Figure 35). Equilibrium experiments also exhibit no correlation of nitrate adsorption to hydrous ferric hydroxide (Figure 36).

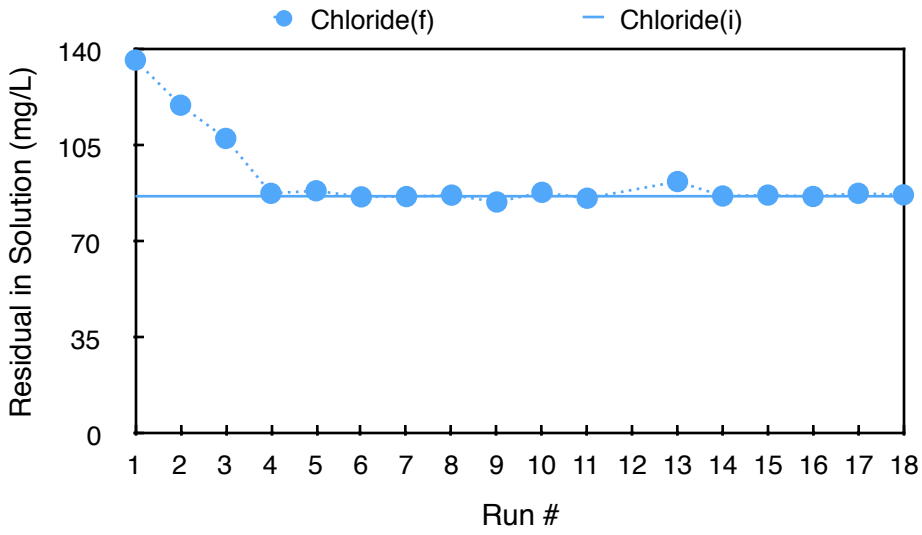

Figure 33. Chloride in adsorption supernatant

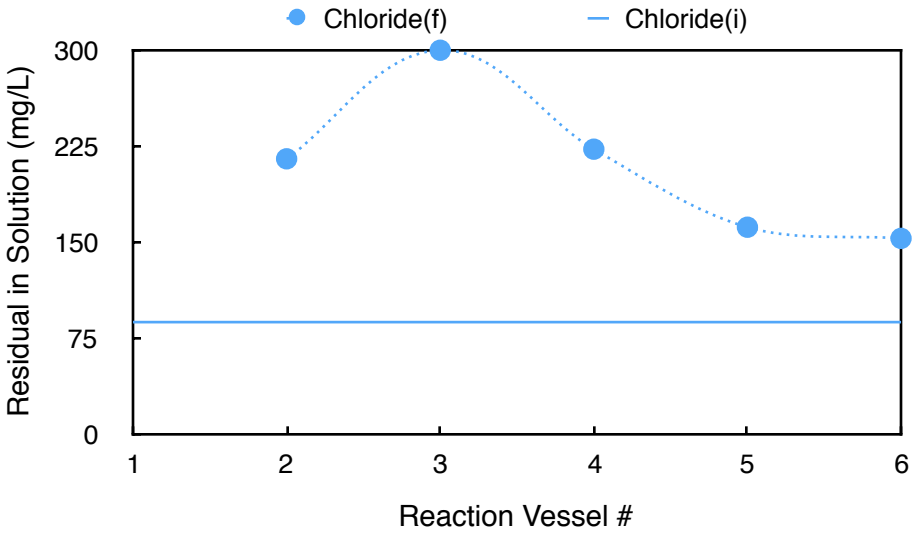

Figure 34. Chloride in adsorption supernatant

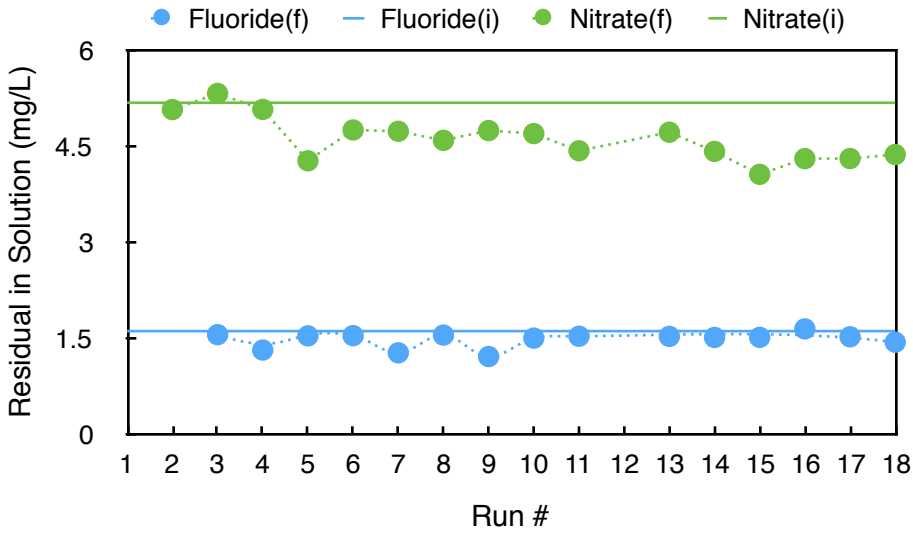

Figure 35. Concentration of fluoride and nitrate in SBR adsorption supernatant

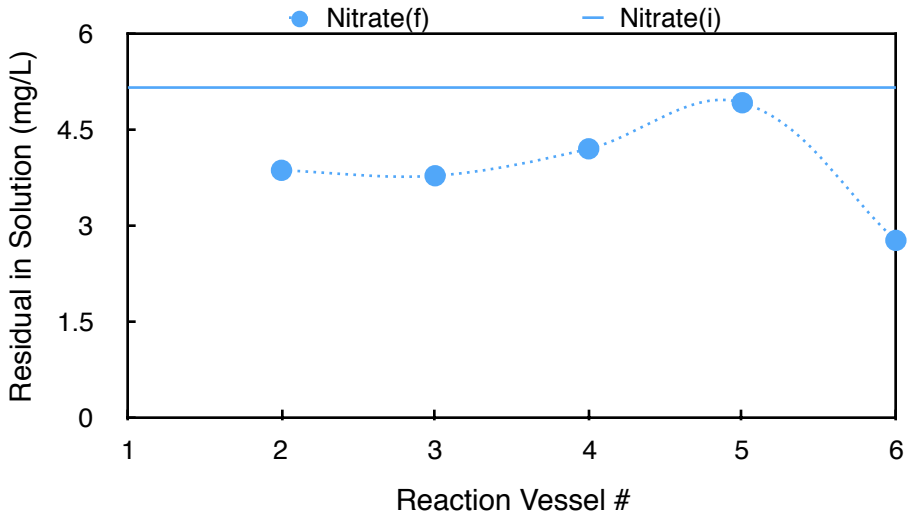

Figure 36. Concentration of fluoride and nitrate in equilibrium adsorption supernatant

XRF Results

Silica loading on the ferric hydroxide adsorbent was characterized by X-ray Fluorescence Spectroscopy. Acid digestion could not be performed due to the formation of volatile SiF_4 in acidic conditions, which would skew total silica count. XRF generated a $\%SiO_2$ mass of 21.42 and $\%Fe_2O_3$ mass of 53.36 on the 18 iteration SBR adsorbent material. Assuming 1 gram of sample, molar amounts were calculated in order to obtain a ratio of silicon to iron in the dehydrated sample Table 7. A total adsorbed ratio of 0.533 mols of silicon per mol of iron resulted. This analytically determined loading coincides well with the loading calculated via mass balance (0.53 molFe/molSi) presented in the data analysis section.

Table 7. XRF Results for SBR Adsorbent material

XRF Results	Mol Calculation	Mol amount of Si & Fe	Si/Fe Ratio
% SiO_2 mass	mmolSiO_2	mmol Si	
0.214	0.0036	0.0036	molSi/molFe
% Fe_2O_3 mass	mmolFe_2O_3	mmol Fe	0.533
0.534	0.0033	0.0067	

XPS Results

XPS results were interpreted by comparison with emission peaks determined in literature in order to understand if polymerization occurred on the SBR adsorbent material. Vempati et al, (1990) published XPS spectra for silica gel, the silicate mineral biotite, silica adsorbed on ferric hydroxide and co-precipitated iron-silicates in their investigation of silica polymerization on hydrous ferric oxide precipitates. Table 8 has results published by Vempati et al., (1990) along with XPS results obtained from the adsorbent material used in the SBR adsorption study.

Table 8. XPS Results compared with published values by Vempati et al., (1990)

XPS Sample	Si(2p) eV	O (1s) Triplet eV		
	Si	O	OH	Si-O
[1]Silica Gel	104	—	—	534.8
[1]Si-free $Fe(OH)_3$	—	530.1	531.8	—
[1] $Fe(OH)_3$ w/ silica ≤ 37.5gSi/kgFe	100.9	530.1	531.6	—
[1] $Fe(OH)_3$ w/ silica ≥ 75gSi/kgFe	101.6, 103.8	530.4	531.9	533.7
[2]SBR $Fe(OH)_3$ 136.7gSi/kgFe	102.5, 103.25	530.5	532	533.5

[1]Experimentl results from Vempati et al., (1990). [2]Experiments Results from this study.

Similarities between the emissions determined by Vempati et al (1990) and the 18-day SBR adsorption media are highlighted by Si 2p and O1s (O, OH, and Si-O) emission peaks. Silica gel has a defined emission for Si 2p at 104 eV, and an O1s (Si-O) peak at 534.8 eV. These peaks are not present on Si-free ferric hydroxide, which only has O binding energies corresponding to 530.1 eV (O) and 531.8 eV (OH). Ferric hydroxide with Si loading below 37.5 gSi/kgFe exhibits O and OH binding energies similar to those

found on virgin ferric hydroxide, along with an Si peak at 100.9 eV, which Vempati et al (1990) attributes to the presence of monomeric adsorbed silica. As the Si loading increases to ≥ 75g Si/kgFe, an Si 2p doublet is formed with peaks at 101.6 eV and 103.8 eV, along with an Si-O peak at 533.7 eV. These binding energies are close enough as those evident in silica gel for Vempati and co-workers (1990) to conclude silica polymerization on the ferric hydroxide surface. The emission for the SBR adsorbent, which has a loading of 136.7 gSi/kgFe, has an Si 2p doublet with peaks at 102.5 eV and 103.25 eV, along with an Si-O peak at 533.5 eV. These binding energies also show similarity to data collected by Vempati et al (1990) for silica gel Si and Si-O binding energies, indicating that surface polymerization is indeed likely.

BET Results

BET analysis resulted in a surface area of 164.5 m^2/g for SBR freeze dried ferric hydroxide adsorbent. As reported by Dzombak and Morel (1990), BET surface area values for dry ferric hydroxide range from 159-306 m^2/g. Variances in surface area measurements may be accounted for by differences in concentration of ferric chloride and NaOH solutions used for precipitation, variances in mixing rate, dehydration method, and experimental error. Surface areas determined from dehydrated samples are significantly lower than those determined by in situ adsorption 400-800 m^2/g or theoretical calculation, 840 m^2/g. Averaging all reported values for ferric hydroxide surface area, Dzombak and Morel (1990) concluded a best estimate for ferric hydroxide surface area in solution to be 600 m^2/g. Hansen and co-workers (1994) found the best fit to their experimental data using a surface area of 600 m^2/g in their model, as opposed to their BET derived surface area of 269m^2/g.

Data Analysis

Mass balance calculations rendered adsorption loading of silicon onto ferric hydroxide for SBR and equilibrium experiments with RO concentrate and SBR experiments with IC coagulation supernatant (Figure 37). Each RO SBR run is comprised of 5, 10, 15, 25, 35, and 60 minute samples. IC SBR runs are comprised of 10, 15, 20, 25 and 30 minute samples. Each increasing sampling time corresponds to decreasing silica concentration in solution and consequently higher silicon to iron ratios. The trend resembles a linear to convex curve, instead of the expected concavity. SBR experiments with RO concentrate eventually reached a final loading of 0.53 molSi/molFe (XFR found 0.533 molSi/molFe) with 5.34% final silica removal. SBR experiments with IC coagulation supernatant were not exercised to completion and therefore do not have an associated final loading. For equilibrium experiments, the lowest silica removal achieved was 12.64%, corresponding to a final loading of 0.47 molSi/molFe. It is important to note that equilibrium experiments did not achieve the same low percentage removal as did the SBR experiments, and likely have more adsorption capacity. Therefore maximum silicon loading between the two is not directly comparable. Silicon loading in SBR experiments, incorporating ±15 & 20% potential error in iron removal with each sampling, and equilibrium final loading are recorded in Table 9.

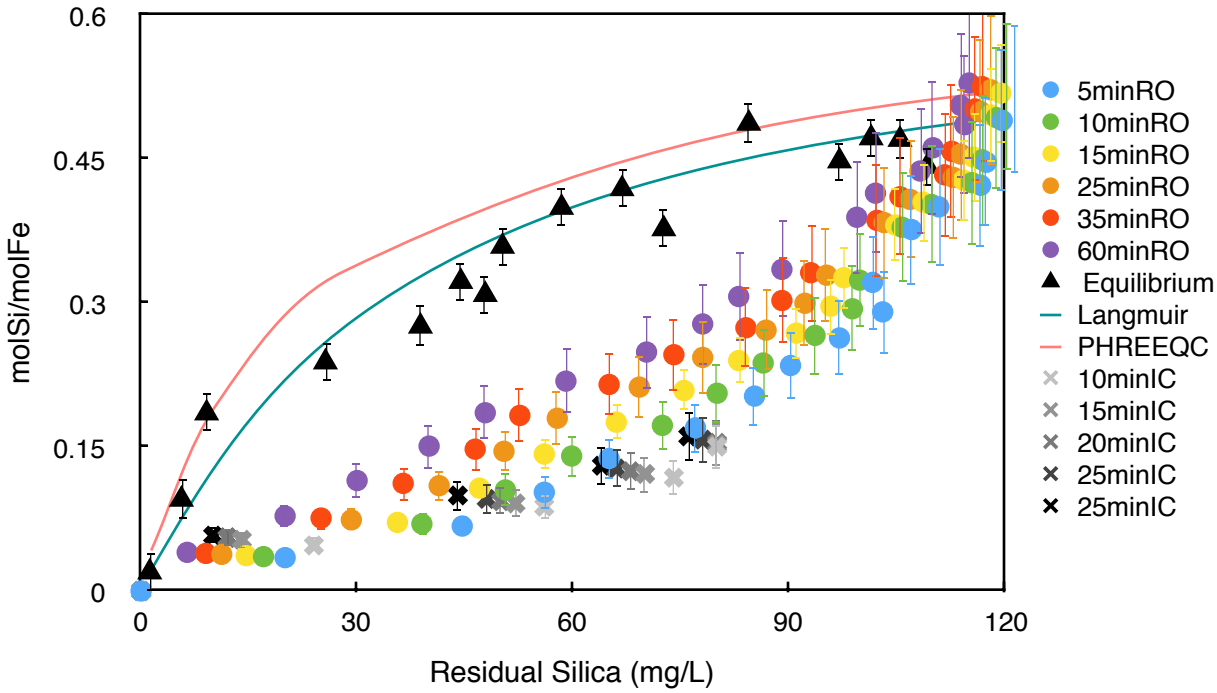

Figure 37. Results of data analysis for SBR and equilibrium adsorption experiments, along with langmuir and PHREEQC adsorption Isotherm models

Table 9. Maximum loading achieved with sbr and equilibrium experiments

Highest Loading Achieved	-20% Fe Removed	-15% Fe Removed	Calculated final loading molSi/molFe	+15% Fe Removed	+20% Fe Removed	Residual Silica concentration (mg/L)
molSi/molFe (RO SBR)	0.48	0.49	0.53	0.58	0.59	115.0
molSi/molFe (RO Equilibrium)	—	—	0.47	—	—	105.4

Adsorption Modeling

Adsorption modeling of the experimentally developed equilibrium adsorption isotherm was investigated using both Langmuir and Freundlich relationships. The Langmuir relationship had the best fit seeing as it incorporates a plateau in adsorption corresponding to q_{max}. Adsorption parameters determined with both models are

Table 10. Adsorption parameters derived from isotherm modeling

Isotherm model	K	qmax / n(Freundlich)
Langmuir 1	0.026	0.65
Langmuir 2	0.024	0.71
Freundlich	0.023	0.68

recorded in Table 10. Surface Complexation Modeling using PHREEQC simulations incorporating dimer adsorption and surface trimerization reactions in accordance to Davis et al., (2002) and Swedlund et al., (2010), respectively, resulted in inconsistencies accounting for total silicon according to the following equation:

(42) $Si_{TOT} \neq H_4SiO_4 + \equiv FeOSi(OH)_3 + \equiv FeOSi_2O(OH)_4^- + \equiv Fe_2H_6Si_3O_{10}$

This is likely due to inability to model these reactions in PHREEQC, or lack of experience with the software. Only complexation reactions involving monomeric silica adsorption appeased the mass balance check, and were therefore used. Monomer adsorption reactions are as follows:

(43) $Si_{TOT} = H_4SiO_4 + \equiv FeOSi(OH)_3$

(44) $\equiv FeOH + H_4SiO_4 \leftrightarrow \equiv FeOSi(OH)_3 + H_2O$ logK 3.6 (Hansen et al, (1994))

(45) $\equiv FeOH + H_3SiO_4^- \leftrightarrow \equiv FeO_2Si(OH)_2^- + H_2O$ logK -6.7 (Davis et al, (2002))

Initial simulations with site densities (N_{s1} and N_{s2}) proposed by Dzombak and Morel (1990), N_{s1}(0.005 mol/molFe) and N_{s2}(0.2 mol/molFe), resulted in significantly less

silicon loading than observed experimentally. Since N_{s1} sites are specific to cation adsorption, they were not altered. N_{s2} sites are attributed to adsorption of neutral and anionic constituents in solution, such as silica, and therefore were adjusted to fit experimental data. As a basis of alteration, total loading from SBR adsorption (0.53 molSi/molFe) was used as a possible reactive site density. The logic behind this was, assuming monolayer coverage, each silica sorbed would consequently correspond to an adsorption site. Using experimentally derived silicon loading (0.53 molSites/molFe) in the DLM simulation did not match experimental values, but was close. The next step was to use the q_{max} as described by the Langmuir isotherm generated form equilibrium adsorption experiments. Using the Langmuir q_{max} and adsorption constants proposed by Hansen et al (1994) and Davis et al (2002), generated a comparable fit of experimental data with the PHREEQC simulation (Figure 37).

Table 11. Adsorbent parameters used in PHREEQC simulation

Origin of values used for Ns2	Ns1(strong)	Ns2(weak)	mol Si/mol Fe
Dzombak and Morel (1990)	0.005	0.2	0.12
SBR Loading Amount	0.005	0.53	0.42
Langmuir q_{max}	0.005	0.65	0.521
Experimentally Determined Loading	—	—	0.53

Regeneration Results

Operating the cell for 24 hours effectively removed all ferric ions from solution as evident by zero resulting current (Figure 38). Solution color also changed from deep brown to completely transparent signifying removal of ferric ions. Characterization of the film deposited on the cathode was not conducted due to lack of time and funding.

With further research, this may prove to be an effective method for regeneration of ferric hydroxide media used in soluble silica sorption or coprecipitation. Economic feasibility may however prove to be a hindering factor.

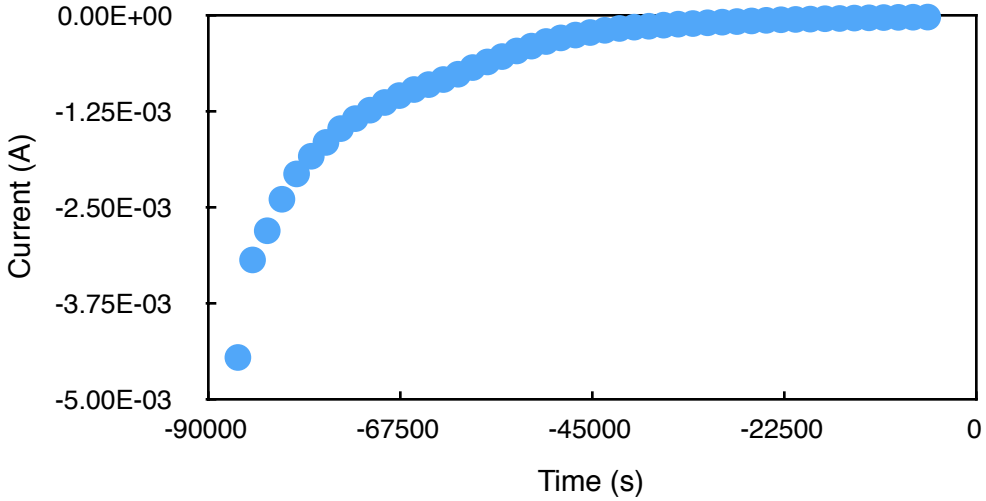

Figure 38. Reduction of current with time due to electrodeposition of ferric ions in solution

Discussion

Coagulation of colloidal silica matter in IC wastewater proved relatively straight forward with ferric chloride. Ferric ions adequately neutralized the silica surface charge allowing flocculation and settling to occur, and also exhibited a range of effective treatment options in regard to pH and dose. IC waste waters have little buffering capacity making them highly susceptible to pH change. Leveraging this, ferric chloride doses were able to rapidly reduce solution pH without the need for additional acid introduction. Lower pH conditions silica particles for neutralization by reducing surface charge accommodating a lower necessary dose of ferric chloride. However, it was also observed that due to lack of buffering, driving solution pH too low rapidly re-stabilized particles with positive zeta potential. Higher doses at constant pH resulted in increased particle size, but did not have a significant impact on reduction in turbidity. Implementation of ferric chloride as a coagulant for silica colloids in IC wastewater is certainly feasible and optimizable by both pH and dose. The mechanism for destabilization of silica colloids in IC wastewater by ferric chloride was determined to be charge neutralization as adsorption to pre-formed ferric hydroxide proved ineffective.

Amorphous ferric hydroxide proved effective for rapid removal of monomeric silica in both IC coagulation supernatant and RO concentrate. Although high doses of ferric hydroxide were used, implementation of the SBR approach showed extended effective utilization of the adsorbent material. With IC coagulation supernatant, ferric hydroxide dosed at 15.4 molFe/molSi achieved 92% silica removal (10 mg/L residual concentration of silica) within 30 minutes at pH 5. For RO concentrate, the initial SBR

dose of 25 molsFe/molSi yielded 94.75% silica removal within 60 minutes (6.4 mg/L residual concentration of silica) at pH 8. After 7 SBR doses of RO concentrate, the total dosing ratio could be considered to be 3.33 molFe/molSi which achieved 67% total silica removal (35.6 mg/L) with a total reaction time of 6 hours at pH 8. Equilibrium adsorption of RO concentrate at 3.33 molFe/molSi resulted in 78.5% silica removal at pH8, but required a total reaction time of 18 days. This study exhibits that silica adsorption by ferric hydroxide can be very rapid and is a highly tunable process by altering pH, dose and reaction time.

ICP-OES results showed a continual but slowly decreasing trend of silica uptake by ferric hydroxide in SBR experiments, along with adsorption of other constituents in solution. Cations like calcium, magnesium and potassium showed rapid initial uptake but adsorption capacity quickly expired within two doses. Ferric hydroxide showed selective affinity for strontium adsorption, with continual capacity until the end of the experiment. This means that strontium likely does not compete with other cations in solution for adsorption and may have species specific sites on the ferric hydroxide surface; similar to calcium (Dzombak and Morel,1990). Arsenic, undetermined to be arsenite or arsenate, showed adsorption to the ferric hydroxide surface, but levels were so low no conclusive trend could be observed. Arsenic removal in water by ferric hydroxide adsorption is notoriously inhibited by silica adsorption (Swedlund, 1998), and was likely outcompeted for adsorption sites by $H_3SiO_4^-$. Iron concentrations in adsorption supernatant were highly sporadic between SBR runs, often non-detectable and never exceeded 0.25 mg/L. This validates the proposed attribute of ferric hydroxide being extremely insoluble in solution, reducing the risk of metal-silicate precipitation as

observed by researchers using magnesium and aluminum hydroxide (Salvador, et al., 2014).

The exact mechanism of silica sorption onto ferric hydroxide cannot be definitively answered in this investigation, however trends elicited by SBR experimentation can certainly provide insight into characteristics of the resulting silica/ iron material. The isotherm profile generated by equilibrium experiments was described well using a Langmuir isotherm, and PHREEQC simulation. The Langmuir adsorption model accounts for a dispersion of sites on the ferric hydroxide surface with a constant adsorption energy between all sites, K_{ads}, indicating what is often considered 'monolayer coverage'. This is reinforced by the PHREEQC simulation which was able to generate an agreeable fit to experimental data using only a monomeric adsorption reaction, although with a reactive site density much larger than published values. In order to get the PHREEQC model to fit, 0.65 molSites/molFe was used for a site density, compared to a value within the range defined by Dzombak and Morel (1990) of 0.1-0.3 molSites/ molFe. Initially, these findings in conjunction seem to point to monolayer, or non-polymerized coverage of silica on the iron surface.

Findings by XRF and adsorption mass balance calculations both agree upon a final loading of 0.53 molSi/molFe for SBR experiments using RO concentrate. This loading is much higher than expected from values published by Dzombak and Morel (1990). In order to achieve 0.53 molSi/molFe loading, either the number of actual reactive sites must have been significantly larger than what has been determined experimentally by the 17 authors cited by Dzombak and Morel (1990), or there is multilayer coverage occurring on the iron surface in the form of silica polymerization.

Assuming the previously published and mutually agreeing values for hydrous ferric oxide site density range between 0.1-0.3 molSites/molFe are correct, this high observed adsorption loading may be explained by surface polymerization. Surface polymerization is certainly supported by both XPS findings and the trend observed of decreased settling rate with increased loading in turbidity experiments. XPS determined Si and Si-O binding energies on the SBR adsorbent material similar to that of silica gel as reported by Vempati and co-workers (1990). This indicates that the silica present on the iron surface is involved in the same bonding as high order polymerized silica; and is therefore itself, polymerized. Decreased settling rate with increased silica loading was determined to be caused by increasing magnitude of particle surface charge, thereby resulting in increased particle stabilization. As previously stated, the pH_{ZPC} of silica was found to be ~2 which coincides well with the literature (Iler, 1979). The pH_{ZPC} of ferric hydroxide was found to be ~8 which also corresponds well with the literature (Dzombak and Morel, 1990). These findings dictate that as the bound silica on the iron surface transforms from monomer to polymer, the particle agglomerate will begin to incur a larger negative charge. This is because, as noted by Iler (1979), the pKa of silica species continually decreases as silica transforms from mononomer (pKa 9.89) to dimer (pKa 8.5) to higher order polymerized species (pKa 6.7). This relationship then results in a negatively charged, ionized surface (M-O-Si-O^-); which was certainly observed here experimentally. The results found in this study strongly suggest silica polymerization occurred during SBR experiments at pH 8, with only theoretical isotherm modeling suggesting monolayer coverage.

These seemingly conflicting result between monolayer and multilayer adsorption may be reconciled by findings published by Swedlund et al., (2010). Swedlund and coworkers (2010) propose that in solutions of high silica concentration, monolayer coverage of silica forms on the hydrous ferric oxide surface followed by the formation of a second silica layer. Through ATR-IR, Swedlund and co-workers (2010) found that the second layer of silica bridges two monomer adsorbed silica molecules on the iron surface. This produces a ratio of 2:1 monolayer:bilayer adsorbed species. A rough expression describing this trend is as follows:

(46) $0.5q_{monolayer} = q_{bilayer}$

(47) $q_{TOT} = q_{monolayer} + q_{bilayer} = q_{monolayer} + 0.5q_{monolayer}$

Optimizing Equation 47 to meet silica loading determined by XRF yields a reactive site density of 0.355 molSites/molFe. This value is higher than the maxima of published values (0.3 molsites/molFe), but certainly not by the substantial amount that was required to generate a fit with the DLM model (0.65 molSites/molFe). The question then becomes, why would an adsorption model expressed with monolayer parameters fit the experimentally determined isotherm data? Theoretically if binding were occurring between silica and the iron surface, it should be at a different energy than silica forming a trimer on the iron surface; and therefore not be able to be modeled with a single adsorption constant K_{ads}. Unfortunately, this study lacks information to properly address this question, but perhaps it may be due to similar energetics in creating Si-O-M bonds and Si-O-Si bonds. This, after-all, is highly reflected in nature with most silicates having trivalent metals exchanged for a silicon atoms within their mineral structure.

As noted earlier, certain principals observed in SBR experiments used for IC and RO silica adsorption may prove useful in designing a ferric hydroxide reactor for silica adsorption. Notably, using an SBR approach allows for complete utilization of the adsorbent material, even when rapid reaction times are used (<60minutes). Extending this observation to a flow through design, the same principal may be leveraged by implementing reactors in series. In this format, incomplete silica removal from higher loaded media could be compensated for by significant silica uptake in less loaded media present in subsequent reactors. In order to segregate high and low loaded ferric hydroxide, characteristics of particle charge and settling velocity could be leveraged. A settling basin could be installed after each flow reactor allowing particles with low loading to settle out and remain in the reactor. High loaded particles would obtain a large negative surface charge and remain in solution. These loaded particles would accumulated and flow out with the process supernatant. Ferric chloride could be used to coagulate these highly loaded particles and isolate them from solution, allowing silica and iron free supernatant to be processed through micro filtration as a final polishing step before reuse. Coagulated $\equiv FeOSi(OH)_3$ could be settled out, removed and potentially regenerated for continual use. Figure 39 represents a theoretical sketch of this described process.

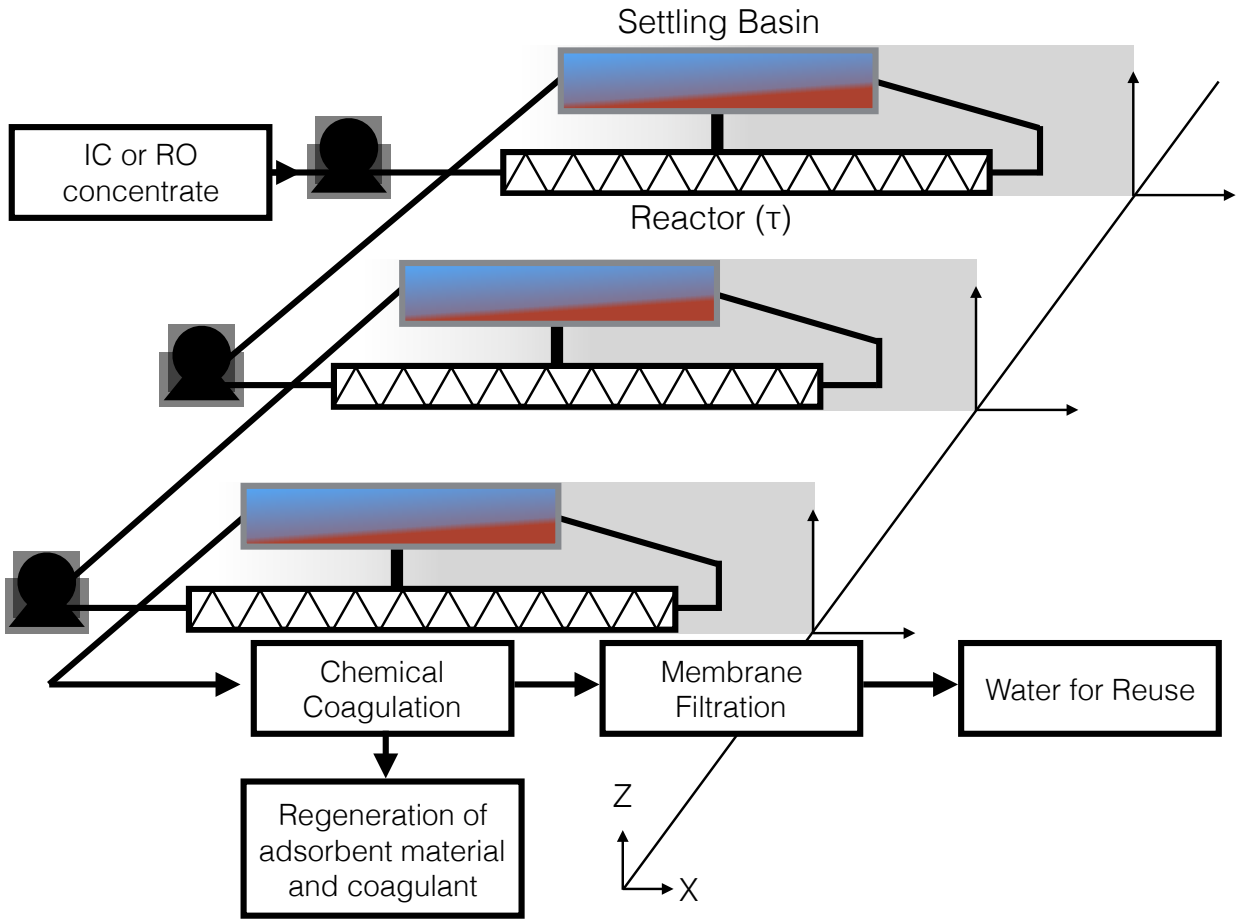

Figure 39. Theoretical proposal for ferric hydroxide reactor to remove silica via adsorption

Conclusion

Thermoelectric, IC, and RO operations all discharge significant amounts of water on a daily basis. Potential for this water to be reused on site, or synergistically in another facility, is hindered by inherent silica concentration. Mitigation practices do not solve this problem as they simply allow for a high silica concentration to be maintained during processing by delaying precipitation, or circumvent the possibility of precipitation by inhibiting allowable recovery in RO. This is achieved by manipulating physiochemical properties of silica such as solubility, speciation, and metal co-precipitation. Silica removal is an alternative approach to silica scale mitigation and would allow uninhibited reuse of wastewater. There is need to develop a robust and cost effective silica removal method that is rapid and has potential to be regeneratable. This study aimed to evaluate the potential of comprehensive colloidal and dissolved silica removal with ferric chloride and ferric hydroxide. The common application of ferric chloride in water treatment in New Mexico, along with it being a precursor to ferric hydroxide, made it an promising candidate to be used in colloidal silica coagulation. Ferric hydroxide has not been evaluated by recent publications for silica removal in industrial wastewater and was chosen for its high affinity for silica sorption and robust insolubility at a variety of pH. Waste streams studied in this work included IC wastewater generated in Hsinchu, Taiwan and RO concentrate generated at the University of New Mexico, USA. Coagulation studies were typical in nature and resulted in a variety of successful dosing options for colloidal silica coagulation at pH 5. The mechanism of silica colloid destabilization by $FeCl_3$ was determined to be charge neutralization, as electrostatic

adsorption did not occur in experiments with ferric hydroxide. Adsorption studies proceeded with both a sequencing batch reactor approach and equilibrium batch studies. The sequencing batch reactor approach was selected as an iterative attempt to fully utilize the adsorbent material to the greatest capacity possible, while subjecting it to limited reaction times. Equilibrium studies were utilized in order to have a tangible contrast to the effectiveness of SBR results. Greater than 90% removal of silica in a rapid timescale (60 minutes) proved achievable with ferric hydroxide. Analysis of adsorption supernatant and $\equiv FeOSi(OH)_3$ material provided insight into the mechanism of silica complexation and parallel adsorption reactions. A Langmuir adsorption relationship as well as surface complexation model in PHREEQC were leveraged to understand the nature of silica adsorption to ferric hydroxide. Although adsorption models point to monolayer adsorption, analytical methods determined that the resulting iron surface after SBR adsorption was likely covered with polymeric silica. This study serves as a benchmark in establishing feasibility of using ferric chloride and ferric hydroxide for comprehensive silica removal, either applied simultaneously or as isolated methods. Characteristics of silica adsorption revealed in this study have implications in reactor design including adsorption kinetics, particle surface charge, and flow through reactor schemes. Expansion of this work will be necessary to fully evaluate if silica removal with these compounds is realistic for industrial application.

Next Steps

Despite having successful silica removal results, there are many areas where this study could be expanded and improved. First and foremost, if further silica removal studies are to be effectively executed, it is pertinent to do so in partnership with a thermoelectric

or desalination facility. This will keep all hypotheses, objectives and experiments confined within the context of an industrially applicable reality. Iterative development of a pilot system could prove interesting if silica removal with ferric hydroxide continues to prove feasible with further testing and evaluation of the material. Regeneration of ferric hydroxide adsorbent would likely enhance economic feasibility and investigating regeneration would be a logical extension of this work. Furthermore, findings in this study allude to expedited adsorption using an SBR reactor compared to an equilibrium reactor. SBR experiments proceeded with a series of 1-hour reaction times and produced slightly less, but comparable silica removal to equilibrium experiments (Figure 25) at each respective dosing ratio. This then raises the question, can maintaining constant concentration of an adsorbate in solution generate a driving force to facilitate optimal adsorption in reduced time-frames? This will require SBR experiments to be executed in conjunction to equilibrium studies with timed sampling.

Citations

1. Benjamin, M. M. (2015). Water chemistry. Long Grove, IL: Waveland Press.

2. Brady, P. V., & Carroll, S. A. (1994). Direct effects of CO2 and temperature on silicate weathering: Possible implications for climate control. Geochimica et Cosmochimica Acta, 58(7), 1853-1856.

3. Bremere, I., Kennedy, M., Mhyio, S., Jaljuli, A., Witkamp, G., & Schippers, J. (2000). Prevention of silica scale in membrane systems: removal of monomer and polymer silica. Desalination, 132(1-3), 89-100.

4. Chan, S. (1989). A review on solubility and polymerization of silica. Geothermics, 18(1-2), 49-56.

5. Chorley, R. J., Dunn, A. J., Beckinsale, R. P., Burt, T. P., Brunsden, D., Cox, N. J., & Goudie, A. (1964). The history of the study of landforms; or, The development of geomorphology. London: Methuen.

6. Chuang, S., Chang, T., Ouyang, C., & Leu, J. (2007). Colloidal silica removal in coagulation processes for wastewater reuse in a high-tech industrial park. Water Science & Technology, 55(1-2), 187.

7. Cob, S. S., Beaupin, C., Hofs, B., Nederlof, M., Harmsen, D., Cornelissen, E., . . . Witkamp, G. (2012). Silica and silicate precipitation as limiting factors in high-recovery reverse osmosis operations. Journal of Membrane Science, 423-424, 1-10.

8. Davis, C. C., Chen, H., & Edwards, M. (2002). Modeling Silica Sorption to Iron Hydroxide. Environmental Science & Technology, 36(4), 582-587.

9. Den, W., & Wang, C. (2008). Removal of silica from brackish water by electrocoagulation pretreatment to prevent fouling of reverse osmosis membranes. Separation and Purification Technology, 59(3), 318-325.

10. Dietzel, M. (2002). Interaction of polysilicic and monosilicic acid with mineral surfaces. Water-Rock Interaction Water Science and Technology Library, 207-235.

11. Dzombak, D. A., & Morel, F. M. (1990). Surface complexation modeling: hydrous ferric oxide. New York: John Wiley & Sons.

12. Eikenberg, J., (1990). On the Problem of Silica Solubility at High pH. Paul Scherrer Institute, Wurenlinger und Villigen, Germany.

13. Egger, A. E. (2017). The Silicate Minerals. Retrieved April 06, 2017, from http://www.visionlearning.com/en/library/Earth-Science/6/The-Silicate-Minerals/140

14. Hansen, H. C., Wetche, T. P., Raulund-Rasmussen, K., & Borggaard, O. K. (1994). Stability Constants for Silicate Adsorbed to Ferrihydrite. Clay Minerals, 29(3), 341-350

15. Howe, K. J., Hand, D. W., Crittenden, J. C., Trussell, R. R., & Tchobanoglous, G. (2012). Principles of water treatment. Hoboken, NJ: John Wiley & Sons.

16. Huang, C., Jiang, W., & Chen, C. (2004). Nano silica removal from IC wastewater by pre-coagulation and microfiltration. Water Science and Technology, 50(12), 133-138.

17. Iler, R.K., (1979). The Chemistry of Silica: Solubility, Polymerization, Colloid and Surface Properties and Biochemistry. John Wiley and Sons, New York, USA.

18. Liu, Y., Tourbin, M., Lachaize, S., & Guiraud, P. (2012). Silica Nanoparticle Separation from Water by Aggregation with AlCl3. Industrial & Engineering Chemistry Research, 51(4),1853-1863.

19. Makrides, A. C., Turner, M., & Slaughter, J. (1980). Condensation of silica from supersaturated silicic acid solutions. Journal of Colloid and Interface Science, 73(2), 345-367.

20. Marshall, W. L., & Chen, C. A. (1982). Amorphous silica solubilities—VI. Postulated sulfate-silicic acid solution complex. Geochimica et Cosmochimica Acta, 46(3), 367-370.

21. Maupin, M.A., Kenny, J.F., Hutson, S.S., Lovelace, J.K., Barber, N.L., and Linsey, K.S., (2014). Estimated use of water in the United States in 2010: U.S. Geological Survey Circular 1405, 56

22. Mckeague, J. A., & Cline, M. G. (1963). Silica In Soil Solutions: Ii. The Adsorption Of Monosilicic Acid By Soil And By Other Substances. Canadian Journal of Soil Science, 43(1), 83-96.

23. Milne, N. A., Oreilly, T., Sanciolo, P., Ostarcevic, E., Beighton, M., Taylor, K., . . . Gray, S. R. (2014). Chemistry of silica scale mitigation for RO desalination with particular reference to remote operations. Water Research, 65, 107-133.

24. Ning, R. Y., Tarquin, A. J., & Balliew, J. E. (2010). Seawater RO treatment of RO concentrate to extreme silica concentrations. Desalination and Water Treatment, 22(1-3), 286-291

25. Okamoto, G., Okura, T., & Goto, K. (1957). Properties of silica in water. Geochimica et Cosmochimica Acta, 12(1-2), 123-132.

26. Sims, M. (2015). Examination of Silica Removal with Solids Recycle for Reverse Osmosis Pretreatment (Unpublished master's thesis). Thesis.

27. Sheikholeslami, R., Al-Mutaz, I., Koo, T., & Young, A. (2001). Pretreatment and the effect of cations and anions on prevention of silica fouling. Desalination, 139(1-3), 83-95.

28. Shipman, J. T., Wilson, J. D., Higgins, C. A., & Torres, O. J. (2016). An introduction to physical science. Boston: Cengage Learning.

29. Sjöberg, S. (1996). Silica in aqueous environments. Journal of Non-Crystalline Solids, 196, 51-57.

30. Swedlund, P. (1999). Adsorption and polymerisation of silicic acid on ferrihydrite, and its effect on arsenic adsorption. Water Research, 33(16), 3413-3422.

31. Swedlund, P. J., Miskelly, G. M., & Mcquillan, A. J. (2010). Silicic Acid Adsorption and Oligomerization at the Ferrihydrite–Water Interface: Interpretation of ATR-IR Spectra Based on a Model Surface Structure. Langmuir, 26(5), 3394-3401.

32. Swedlund, P. J., Sivaloganathan, S., Miskelly, G. M., & Waterhouse, G. I. (2011). Assessing the role of silicate polymerization on metal oxyhydroxide surfaces using X-ray photoelectron spectroscopy. Chemical Geology, 285(1-4), 62-69.

33. Swedlund, P. J., & Webster, J. G. (1999). Adsorption and polymerisation of silicic acid on ferrihydrite, and its effect on arsenic adsorption. Water Research, 33(16), 3413-3422.

34. Yokoyama, T., Nakazato, T., & Tarutani, T. (1980). Polymerization of Silicic Acid Adsorbed on Iron(III) Hydroxide. Bulletin of the Chemical Society of Japan, 53(4), 850-853.

35. Vempati, R. K., Loeppert, R. H., Dufner, D. C., & Cocke, D. L. (1990). X-ray Photoelectron Spectroscopy as a Tool to Differentiate Silicon-Bonding State in Amorphous Iron Oxides. Soil Science Society of America Journal, 54(3), 695.

36. Weitz, C. (2016, April 8). Intel Water Facilities Tour [Personal interview]